Additive Functionalization and Embroidery for Manufacturing Wearable and Washable Textile Supercapacitors

*Qiyao Huang, Dongrui Wang, Hong Hu, Jian Shang, Jian Chang, Chuan Xie, Yu Yang, Xavier Lepró, Ray H. Baughman, Zijian Zheng**

Dr. Qiyao Huang, Prof. Dongrui Wang, Dr. Hong Hu, Jian Shang, Dr. Jian Chang, Chuan Xie, Dr. Yu Yang, Prof. Zijian Zheng
Laboratory for Advanced Interfacial Materials and Devices, Research Center for Smart Wearable Technology, Institute of Textiles and Clothing, The Hong Kong Polytechnic University, Hong Kong SAR, China
E-mail: tczzheng@polyu.edu.hk

Dr. Xavier Lepró, Prof. Ray H. Baughman
The Alan G. MacDiarmid NanoTech Institute, University of Texas at Dallas, Richardson, Texas 75083, USA

Keywords: electronic textiles, supercapacitor, additive manufacturing, embroidery, wearable electronics

Electronic textiles require rechargeable power sources that are highly integrated with textiles and garments, thereby providing outstanding durability and washability. In contrast, present power sources fabricated using conventional ex-situ strategies are difficult to integrate with clothing and can degrade during garment washing. Here, a new manufacturing strategy named additive functionalization and embroidery manufacturing (AFEM) is reported, which enables textile-based supercapacitors (TSCs) to be directly fabricated on woven, knitted, and non-woven fabrics. The additive principle of AFEM allows developing TSCs with different types of electrode materials, device architectures, pattern designs, and array connections. High-machine-speed, programmable-design industrial embroidering equipment is used to fabricate TSCs with high areal energy storage and power capabilities, which are retained during many cycles of severe mechanical deformation and industrial laundering with waterproof encapsulation.

1. Introduction

Electronic textiles (E-textiles) have gained increasing attention in recent years due to their enormous application potential in future wearable electronics for healthcare, communication, robotics, fashion, protective garments, and engineering textiles. In the past decade, remarkable progress has been made in developing novel wearable materials for E-textiles with a wide variety of functionalities.[1-3] A common and indispensable element to achieve high-performance E-textiles is a reliable wearable power supply, which not only provides satisfactory energy storage and power delivery capabilities but also is highly flexible, lightweight, waterproof and even washable.[4-6] Textile-based supercapacitors (TSCs), supercapacitors built with textile fibers, yarns, and fabrics, appear to be very promising candidates because of the textile's mechanical softness and durability.[7-10] When compared with planar thin films, the fibrous structure and three-dimensional textile configuration of TSCs provide advantages for achieving high electrochemical capacitance and stability.[11-12]

Most TSCs reported to date are fabricated using conventional manufacturing strategies, where each TSC is firstly fabricated ex-situ with a ply-yarn or multilayer-fabric structure and then integrated into the E-textile circuit by using weaving, knitting or lamination technologies (**Figure S1a** and S1b).[11-17] Although such an "attach to" strategy can yield high-performance devices, it is complicated to integrate the TSCs with functional E-textiles using external interconnects. In addition, the weaving and knitting processes often involve high tensile and tearing stresses during the interlacing and interlocking of electrode yarns, which can degrade TSC performance. To address these integration issues, several recent reports tried to directly fabricate TSCs through lithographic patterning and/or printing of electrode materials on fabrics (Figure S1c),[18-24] which provided greater flexibility in device integration with external electronic parts. However, this strategy requires a multi-step patterning process on rough fabric

surfaces, which is technically challenging for practical manufacturing and is limited to the fabrication of in-plane micro-devices.

In addition to fabrication and integration issues, washability is also a serious obstacle to the real application of these TSCs. High tension, shearing, and abrasion stresses that occur during washing can destroy the contacts between the textile surfaces and the deposited materials. As a result, the multilayer structures of the TSCs can become unstable after cycles of washing, which leads to permanent device damage. Recently, encapsulation with waterproof materials such as silicone rubber, polypropylene, and poly(ethylene terephthalate) has been employed to protect textile devices from external impacts such as stretch and water.[24-29] However, only a few devices could survive multiple cycles of washings under commercial laundry conditions.[28-29]

In this paper, we report a new strategy named additive functionalization and embroidery manufacturing (AFEM), which enables seamless design-on-demand fabrication and integration of TSCs onto different types of textile fabrics, and at the same time provides excellent wearing and washing durability. AFEM starts from the additive functionalization of textile yarns into composite electrode yarns by successively depositing various functional materials on yarn surfaces, and then utilizes the additive manufacturing process of embroidery to directly configure the composite electrode yarns into desirable shapes, structures, and connections of TSCs on any textile surfaces (Figure 1, Movie S1), followed by waterproof encapsulation. The key advantages of AFEM are its simplicity to simultaneously combine device fabrication and integration in one step, its compatibility with a wide variety of TSC materials and structures, and the provided durability during use and washing. Here, we demonstrate the versatility of AFEM with (1) the additive functionalization of composite electrode yarns with different

electrode materials; (2) the additive embroidery manufacturing of two major device structures, including laterally patterned in-plane TSCs and vertically stacked out-of-plane TSCs; and (3) the direct fabrication of TSCs on vastly different textiles, including woven, knitted, non-woven, and stretchable fabrics. We study the electrochemical characteristics of the TSCs and show their unprecedented stability for different wearing conditions and even after repeating washes with a standard AATCC (American Association of Textile Chemists and Colorists) laundry process.

2. Results and Discussion

In AFEM, conventional textile yarns are firstly functionalized into composite electrode yarns (Figure 1a, Step 1 and 2). In a typical experiment, ~500 nm thick nickel (Ni) was firstly deposited on conventional cotton yarns using a polymer-assisted metal deposition (PAMD) method we previously developed, to yield Ni-coated cotton (Ni-Cotton) yarns (Figure S2a).[30-32] Ni was coated uniformly on the fiber surfaces and the as-prepared Ni-Cotton yarn provided a low linear resistance of 0.88 Ω cm^{-1} with a bulk electrical conductivity of approximately 333 S cm^{-1} (Figure 2a and S2b). The Ni-Cotton yarns were then coated with reduced graphene oxide (RGO) by electrochemical deposition to form the composite electrode yarns (denoted as ERGO/Ni-Cotton) (Figure 2b, Figure S2c).[11] The composite electrode yarns exhibited a decent electrical conductivity of about 84 S cm^{-1} (linear resistance: 3.91 Ω cm^{-1}) while well retained the textile-like flexibility and durability: after 5,000 cycles of bending, the electrical resistance only changed by 16% (Figure S2d). Compared to the pristine cotton yarns, they maintained a similar maximum load with a significant increase in the breaking extension from 7% to 10%, which provided adequate mechanical characteristics for embroidery (Figure 2c and Table S1).

The composite electrode yarns were next embroidered onto the textile fabric. In order to minimize the abrasion of the materials during embroidery, the composite electrode yarns were laid flat on the targeted fabric substrate and fastened with non-conducting fixing yarns (Figure 1a, Step 3) to form patterns. Afterward, stainless steel yarns were embroidered over the edges of the composite electrodes to serve as conductive leads for testing or connecting with other electronic parts. Finally, an aqueous electrolyte was printed on the electrode area and the entire device was encapsulated with Ecoflex silicone rubber. Because of the high flexibility and transparency of Ecoflex, this coating provides good waterproof ability without deteriorating the aesthetics of the textile and the mechanical properties of the device electrodes.[33] Taking advantage of the flexibility of the embroidery technique, AFEM can fabricate devices with vastly different structures on a wide range of textiles, including woven, knitted, non-woven, and even stretchable fabrics (Figure 1b).

Compared to the well-known knitting and weaving methods that have been widely applied for the integration of fiber/yarn-shaped TSCs, the newly reported additive embroidery approach can effectively reduce the harsh mechanical deformations of electrode yarns. We conducted Scotch tape peeling tests on the composite electrode yarns. After peeling the tape off, the degree of the removal of active materials from the yarn was inspected, which can be an indicator of the abrasion resistance of the electrode. RGO sheets on the surface of Ni-Cotton were peeled off by the Scotch tape in the peeling test, while the sheets between the fiber gaps within the yarn were not affected (Figure S3a-c). The result shows that the adhesion between RGO sheets and Ni is not high, which is attributed to the relatively weak bonding between RGO sheets and Ni-Cotton. The low adhesion prohibits the fabrication of TSCs with conventional knitting and weaving methods. In the traditional weaving and knitting processes, composite electrode yarns need to be interlaced or interlocked for the formation of fabric structures (Movie S2). As a

result, electrode yarns have to suffer the abrasion and tension during the processes, leading to the crack and fall off of coated materials from yarn surfaces (Figure S3d-S3i). On the contrary, in the additive manufacturing process of embroidery, composite electrode yarns do not need to run through every stitch or form loops with a high degree of deformation. They are only laid on the existing fabric surfaces and then fixed by additional non-conductive fixing threads. Therefore, after undergoing the embroidery process, composite electrode yarns could retain the coating surface and its linear resistance only showed about a 3% increase (Figure S3j-k). As such, this additive embroidery method can be compatible with a variety of electrode materials, device structures, and fabric substrates.

Composite electrodes can be positioned in pairs either on one side or on both sides of the fabric substrate to develop in-plane TSCs with the laterally interdigitated electrode structure or out-of-plane TSCs with the vertically stacked structure (Figure 2d). Figure 2e shows the in-plane TSC consisting of two pairs of interdigitated finger electrodes on a piece of cotton fabric, where the gap distance between the opposite electrodes was ~1 mm. In such a device, the non-conducting fixing yarns only acted as the separators to avoid electrical shorts between opposite electrodes without contributing to the electrochemical reaction of the TSC. Whereas in the out-of-plane TSC, the cotton fabric was sandwiched by the two opposite electrodes, each of which was comprised of four composite electrode yarns (Figure 2f). The cotton fabric in such a vertically stacked structure served as not only the supporting substrate but also the separator of the TSC. As such, the number of finger electrodes of the out-of-plane TSC on the same projection area was twice that of the in-plane TSC.

We studied the electrochemical properties of these embroidered ERGO/Ni-Cotton TSCs in a gel electrolyte made of polyvinyl alcohol (PVA) and LiCl (PVA/LiCl). Cyclic voltammetry

(CV) curves of the in-plane TSC maintained rectangular shapes with increasing scan rates from 10 mV s^{-1} to 2 V s^{-1}, exhibiting their typical double electric layer capacitive property (Figure 3a). Nearly symmetric triangular shapes with small internal resistance (iR) drops of 47 mV and Coulombic efficiency of ~95% at the current density of 1 mA cm^{-2} were observed in the galvanostatic charge/discharge (GCD) curves, indicating the typical electrical double-layer capacitor behavior and the good electrical conductivity of the electrode yarns (Figure 3b). The areal capacitance calculated from the CV curve at the scan rate of 10 mV s^{-1} was 5.34 mF cm^{-2}, of which as much as 1.60 mF cm^{-2} was retained when the scan rate was dramatically increased to 2 V s^{-1}. This in-plane TSC exhibited stable cycling performance, corresponding to 97% capacitance retention after 10,000 charge/discharge cycles (Figure 3c).

For the out-of-plane device, the number of pairs of composite electrode yarns on the same device area was twice as that of the in-plane device. Both GCD and CV curves of the out-of-plane TSC showed double-layer capacitive behavior similar to the in-plane TSC (Figure 3d and S4a-c). The out-of-plane TSC showed a smaller iR drop (23 mV at the current density of 1 mA cm^{-2}), and its areal capacitance was slightly more than double that of the in-plane TSC (Figure 3e). Such capacitive enhancement of the out-of-plane TSC was attributed to both the increase in the number of finger electrodes and a smaller internal resistance, which was confirmed by the AC impedance spectra (Figure S3d). The equivalent series resistance derived from the Z' intercept of the Nyquist plot describes the total resistance originated from the gel-electrolyte, the electrode, and the contacts.[16, 34] The out-of-plan TSC displayed a smaller equivalent series resistance of 11.8 Ω than the in-plane device (Figure S5). The distance between opposite electrodes (i.e., the thickness of fabric substrate) for the out-of-plane TSC (~450 μm) was shorter than for the in-plane TSC (~1 mm) in this demonstration. This shorter separation distance could effectively decrease the internal resistance of the device and increase the rate of

ionic diffusion between opposite electrodes, which led to the enhancement of the capacitance obtained at a specified charging rate.

Importantly, AFEM is applicable to various types of electrode materials and electrolytes. To demonstrate its versatility, we fabricated two other in-plane TSCs with the same device structure but using different composite electrode yarns, namely multi-walled carbon nanotube-wrapped Ni-Cotton (MWNT/Ni-Cotton) and RGO-dip-coated Ni-Cotton (DRGO/Ni-Cotton) with PVA/LiCl. These TSCs also exhibited typical double-layer capacitive behavior (Table 1, Figure S6 and S7). Their specific areal capacitances were 15.75 mF cm^{-2} and 11.38 mF cm^{-2}, respectively, at the scan rate of 10 mV s^{-1}. We also replaced PVA/LiCl with bis(trifluoromethylsulfonyl)amine lithium salt (LiTFSI), which significantly extended the voltage window of the device from 0.8 V to up to 1.5 V (Table 1 and Figure S8a-c).[35-36] The electrochemical characteristics of these embroidered TSCs are similar to the best-performing in-plane supercapacitors fabricated by conventional lithographic processing and mask-assisted material deposition methods (Table S2, Figure 3f, and Figure S8d).[21-23, 26, 33, 37-38]

More importantly, benefiting from the purely additive process of AFEM, the structure, shape, and connection of TSCs can be tailored according to the demands of different applications. For example, one can tune device capacitance by adjusting the total effective electrode length. As a proof-of-concept, we embroidered TSCs with one pair of composite electrode yarns of different electrode lengths (L-TSC) or with multiple pairs of electrode yarns of the same electrode length (I-TSC) (Figure 4a). Both methods resulted in a linear increase of the device capacitance as a function of the total electrode length. However, I-TSC exhibited a more prominent capacitive enhancement than L-TSC, and AC impedance spectra in Figure S9 showed that I-TSC had a much smaller internal resistance compared to the L-TSC with the

same electrode length. This may be because the parallel connection of subunits in I-TSC could effectively facilitate the charge transport inside the shorter finger electrode, resulting in a decrease in the device's internal resistance and improvement of the device capacitance. Besides, the interaction of the opposite finger electrodes between the adjacent subunits could also contribute to the device capacitance.[39-40] According to the working mechanism of electric double layer capacitors (EDLCs), electron charges are distributed on the surface of the opposite electrode. In L-TSC, the electron charges are only distributed on the inner surface of the electrodes. Whereas in I-TSC, the parallel connection with interdigitated electrode configuration enables the electron charges to distribute on both inside and outside surfaces (except for the leftmost/rightmost electrodes as displayed in the inset of Figure 4a). As a result, for the same length and gap distance of electrodes, the effective surface area of I-TSC will be larger than that of L-TSC. Considering the fundamental formula that determines the capacitance of a capacitor: $C=\varepsilon(S/d)$, *where C is the capacitance of the device, ε is the permittivity of the dielectric material being used, S is the surface area of the electrode, and d is the distance between the opposite electrodes, the larger surface area can lead to higher capacitance.*[39] *Therefore, I-TSC could have more prominent capacitance enhancement than L-TSC.* Furthermore, we could also increase the areal capacitance by increasing the embroidery density of the finger electrodes (i.e., the total length of the electrode yarns embroidered on the specific projection area of the fabric). As shown in Figure 4b, the areal capacitance of TSC shows a 6-fold increase when the electrode density is increased by 600%. Also, increasing the size of the electrodes (i.e, the diameter of the composite electrode yarns) can benefit the enhancement of specific capacitance. From the perspective of the AFEM fabrication process, there are essentially no limitations on the size of the electrode yarns. We plied different numbers of yarns to create the ply electrode yarns with different diameters, and respectively embroidered them into in-plane TSCs. The specific capacitance of the devices could linearly

increase with the increase of the ply number (Figure 4c). In addition, we could readily tune the output voltage and current density by connecting an array of TSCs in series or parallel configurations through the embroidery of interconnecting conductive yarns (Figure 4d and 4e). We embroidered 16 in-plane TSCs, each showing a typical voltage window of 0.8 V and a capacitance of ~2.5 mF. Four devices in each column were connected in series and the 4 columns were connected in parallel. Consequently, the voltage output was extended to 3.2 V and the stored energy was enhanced 22 fold (Figure 4f and 4g).

To demonstrate the applicability of AFEM for E-textiles, we embroidered eight TSCs in the shape of four letters "AiMD" on a cotton T-shirt (Figure 5a). These TSCs were connected in series and parallel to achieve an output voltage of 3.2 V, so as to power a light-emitting diode (LED) embroidered as part of the letter "i" (Figure 5b and 5c). Owning to the flexibility of composite electrode yarns, T-shirt embroidered with TSCs could remain good flexibility and softness. The capacitance of the E-textile was well maintained when the T-shirt was rolled, twisted or even immersed in water (Figure 5d). The E-textile showed capacitive retention of 94% after being bent for 4,000 cycles and 97% after being continuously operated underwater for 9 h (Fig. 5e). In addition, we demonstrated that AFEM approach can be applied to various kinds of textile substrates including woven, knitted, non-woven fabrics and even stretchable fabrics (Figure 1b). As a proof of concept, in-plane TSC in the shape of the letter "M" was embroidered onto the stretchable knitted fabric. When the fabric was stretched up to 35% strain, the TSC could remain a relatively stable capacitive performance (Figure 5f). The device also has excellent thermal safety. We conducted a combustion test. Notably, the fire gradually extinguished without further burning when it was approaching the TSC area (Figure S10a and S10b). The coating of gel electrolyte around the device area could account for such extinguishment. When the fire was applied onto the device area that was coated with the gel

electrolyte, no combustion was observed. And the capacitance decayed slowly with the increase of combustion time (Figure S10c), which was mainly attributed to the evaporation of water in the gel electrolyte. This result demonstrated that the introduction of such embroidered TSCs, which was made of carbon-based electrode materials, metal-based current collectors and aqueous electrolyte, would not cause additional risk to the fabric substrates, indicating their promise in serving as power devices for E-textile garments.

Most importantly, these TSCs can be machine washable after being encapsulated by waterproof materials, Ecoflex (Figure S11a). We tested the washability in a laundry machine using AATCC Test Method 135. The capacitance retained 50% of the original value after 20 cycles of machine washing and drying (Figure 5f). This might be because strong abrasion between TSCs and laundering ballast pieces (cotton fabrics) during the laundry with the high-speed spinning process (500 rpm) led to the damage to the Ecoflex film coated on the TSC area, resulting in a small amount of leakage of the electrolyte and decrease in the capacitive performance (Figure S11b and S11c). This washability can be further enhanced by laminating a waterproof thermoplastic polyurethane (TPU) fabric, where the TPU fabric could not only sustain the waterproof ability (Figure S11d) but also provide an additional protective layer for the Ecoflex film by reducing the abrasion between them and ballast pieces. As shown in Figure 5g and 5h, the TSC can be washed for 20 cycles without an obvious change in capacitance. To our best knowledge, this is the first report of fully wearable and machine-washable supercapacitors. This exceptional washability is attributed to both the encapsulation and the structural stability of the TSC device under deformation.

Finite element simulations further reveal the detail distribution of stress applied to TSC electrodes. Two models were studied. Model I mimicked the multi-layered structures of

electrodes directly coated on the fabric surface in the conventional fabrication of TSCs (Figure 6a), whereas Model II studied the embroidered electrode structure by AFEM (Figure 6b). The detailed modeling and simulation are described in the experimental section. When bent, localized von Mises stress concentration was observed on the electrode surface in Model I (Figure 6c). Such tension stress built up with the increase in the bending curvature, i.e., decrease in the radius of curvature, and finally led to the fracture of the electrode materials (Figure 6c and 6e). In contrast, electrode materials in the AFEM electrode model (Model II) did not show obvious fractures under the bending conditions (Figure 6f). Instead of fracture of the electrode, only small cracks were observed on the upper surface (Figure 6g and 6h). Overall, the composite electrode yarn could well maintain its structure upon the increase in the bending curvature, which was attributed to the fibrous configuration of the yarns and the existence of fixing yarns. The composite configuration of the yarn electrodes of AFEM could release the stress concentration during bending and thus avoid the fracture of the electrode. As a result, AFEM-fabricated TSCs possess high electrical and electrochemical stability under severe mechanical deformations during bending, twisting, stretching, and washing.

3. Conclusion

In summary, AFEM is an important new strategy for the fabrication of wearable and washable TSCs. AFEM outperforms conventional fabrication methods in the following aspects. Firstly, AFEM follows an additive manufacturing principle, where functional materials are successively loaded on the targeting substrate. Specifically, conductive metal layers and electrochemically active materials are firstly loaded onto pristine textile yarns to form composite electrode yarns, and then the composite electrode yarns are added onto the fabric substrate by an additive manufacturing process of embroidery to achieve the assembly of a device. Finally, the device area is encapsulated by adding a waterproof package to enhance the

device's washing fastness. Such an entire process follows the "fabrication-on-demand" principle of additive manufacturing technologies, which can effectively avoid the use of sacrificial materials or expensive masks that are required in the subtractive lithographic methods for making in-plane TSCs. As a result, the manufacturing process is significantly simplified and cost-effective. Secondly, unlike the integration of TSCs by weaving, knitting and stitching technologies reported in the literature, AFEM avoids serious material abrasion and tension during both device assembly and integration, and composite electrode yarns can be well prevented from the harsh mechanical deformation. In AFEM approach, the composite electrode yarns are only laid on the fabric surface and fixed by additional fixing yarns, therefore, high tensile extension or surface abrasion induced by the processing technology can be largely reduced. This advantage provides remarkable device stability in different wearing conditions such as bending and twisting, and more importantly, remarkable washability with appropriate waterproof encapsulation. Last but not the least, AFEM is a mild strategy that can be applied to different sizes of yarns, electrode materials, and electrolytes, which can provide great flexibility for functional and structural designs without affecting the softness and aesthetic of fabrics and garments. TSCs with different shapes, device structures, and capacity specifications can be easily tailor-made onto any fabric using AFEM. Further exploration of material compositions can be used to improve the already attractive electrochemical performance of such embroidered devices. Since fully-automatic embroidery equipment has already been developed in the textile industry, AFEM has a high potential for scalable manufacturing of a wide range of E-textiles in the near future.

4. Experimental Section

Fabrication of Conductive Ni-Cotton Yarns by PAMD: Pristine cotton yarns were washed with deionized (DI) water and ethanol solution, and then were dried at 80 ºC before the PAMD

process. A typical PAMD process for fabricating Ni-Cotton yarns included four steps, namely silanization, polymerization, ion exchange for activation, and electroless deposition (ELD) of Ni. Firstly, cotton yarns were immersed in a 4 % (v/v) [3-(methacryloyloxy) propyl] trimethoxysilane solution (solvent: ethanol, DI water, and acetic acid with a volume ratio of 95:4:1) for 1 h. Afterward, the silane-modified cotton yarns were rinsed with DI water and immersed in an aqueous solution of [2-(methacryloyloxy) ethyl] trimethyl ammonium chloride (METAC) (20 wt%) with potassium persulfate for free-radical polymerization at 80 ºC for 1 h, followed by thorough rinsing with DI water. After that, the PMETAC-grafted cotton yarns were immersed in the catalytic solution, 5 mM ammonium tetrachloropalladate (II) ($(NH_4)_2PdCl_4$), for 30 min at room temperature. Then the treated cotton yarns were rinsed with DI water to remove the excess catalytic ions. Finally, the catalysis-loaded yarns were immersed in the Ni plating bath to perform the ELD process at room temperature. The Ni plating solution was prepared by mixing solution A (Ni stock) and solution B (reductant stock) with a volume ratio of 10:1. Solution A contained $Ni_2SO_4 \cdot 5H_2O$ (200 g L^{-1}), sodium citrate (100 g L^{-1}), and lactic acid (50 g L^{-1}) in DI water (pH = 7.5). Solution B was an aqueous solution of dimethylamine borane (15 g L^{-1}). After 90-min deposition, Ni-Cotton yarns were obtained, which were then washed thoroughly with DI water and dried in air.

Preparation of Composite Electrode Yarns: For ERGO/Ni-Cotton, 3 mg mL^{-1} graphene oxide (GO) aqueous suspension with 0.1 M $LiClO_4$ was prepared as the electrolyte solution. Ni-Cotton yarn was directly used as the working electrode, while Pt wire and Ag/AgCl (3M KCl) were used as counter and reference electrodes, respectively. The electrochemical deposition of GO on the Ni-Cotton yarns was carried out at a constant potential of -1.2 V for 10 min. The GO was further reduced by hydrazine vapor for 5 h at 70ºC. For MWNT/Ni-Cotton, MWNT forest with vertically aligned carbon nanotube arrays was grown on Si wafer by a chemical

vapor deposition method.[41] Two ends of the Ni-Cotton yarn were fixed onto the spinning loom. A layer of thin MWNT sheet with a width of 1.5 cm was continuously drawn from the MWNT forest and then was carefully wrapped on the yarn surface (Fig. S4a). Forty layers of MWNT sheets were wrapped around the Ni-Cotton yarn. Ethanol was then dropped onto the yarn surface to provide surface-tension-based densification, which enables the MWNT sheets to be firmly bound to the Ni-Cotton yarn. For DRGO/Ni-Cotton, the Ni-Cotton yarn was dipped into a 2 mg mL^{-1} GO suspension for 5 min and then was removed for drying at 80 ºC for 10 min. This dip-and-dry process was repeated 5 times. After that, excess GO sheets were washed away, followed by the reduction of GO using hydrazine vapor for 5 h at 70 ºC. The mass loading of carbonaceous materials on each type of composite electrode yarns are presented in Table S3.

Assembly of TSCs via the AFEM Approach: Composite electrode yarns (weight: 2~2.5 mg cm^{-1}) were laid flat on the surface of the fabric and then fastened with additional non-conductive yarn (fixing yarn). In-plane or out-of-plane TSCs were obtained by embroidering pairs of electrode yarns in parallel arrangement on one side or both sides of the fabric. Subsequently, stainless steel yarns were stitched over the edges of the electrodes to serve as conductive leads. The electrolyte was then cast on the device area. The weight of as-assembled in-plane and out-of-plane TSCs were about 160 mg cm^{-2} and 200 mg cm^{-2}, respectively, including the weight of composite electrode yarns, fixing yarns, electrode lead, and gel electrolyte. For the demonstrations, two types of aqueous electrolytes were applied, namely PVA/LiCl and LiTFSI. PVA/LiCl gel electrolyte was obtained by mixing LiCl (6.3 g) with PVA (3 g) in 30 mL DI water. Heating at 85ºC for 1 h under constant stirring facilitated the dissolution process. The ionic conductivity of PVA/LiCl is about 1.3×10^{-3} S cm^{-1} at room temperature. Concentrated LiTFSI aqueous electrolyte with a molality of 5 m or 20 m was prepared by dissolving 5 mol or 20 mol of LiTFSI in 1 kg water, respectively. The ionic conductivity of 5m LiTFSI and 20m

LiTFSI were 0.6×10^{-3} S cm^{-1} and 0.4×10^{-3} S cm^{-1}, respectively. The ionic conductivity of electrolyte *(σ)* was determined by the AC impedance measurement with a frequency of 0.1-100 kHz and an amplitude of 5mV on a CHI600E electrochemical workstation. The ionic conductivity (*σ) is calculated by the equation:* $\sigma = L / (R \times A)$. L is the distance between the two stainless steel plates (i.e. the thickness of the separator), *R* is the resistance obtained from the AC impedance spectrum, and *A* is the contact area of electrodes with electrolyte during the experiments.

Encapsulation of TSC for Waterproofing and Washability: Both sides of the device area were coated with a mixture of Ecoflex™ 00-30 prepolymer and its curing agent (mixing weight ratio: 1/1), followed by curing in the air. To further enhance washability, TSC encapsulated with Ecoflex was encased by waterproof TPU-coated nylon fabrics using an ultrasound welding machine.

Characterization: SEM (JEOL JSM 6490) was used to observe the surface morphology of the Ni-Cotton yarns, the composite electrode yarns, and the configurations of TSCs. The linear resistance of the Ni-Cotton yarn and as-made composite electrode yarns was measured by a source meter (Keithley 2400). An Instron 5566 was used to evaluate the tensile properties of the yarns. A KES-FB2 (Kato Tech Co., Ltd.) bending tester was used to conduct bending tests on the yarns. A TEM (JEOL JEM 2011) was used to study the structure of the MWNT nanofibers drawn from the MWNT forest. Raman spectroscopy with a 514 nm laser was used to study the GO sheets before and after reduction. For the electrochemical performance evaluation of the as-made TSCs, CV, GCD, and AC impedance spectroscopy measurements were performed on a CHI600E electrochemical workstation. The impedance spectra were recorded by applying a sine wave with 5 mV amplitude over a frequency range from 100 kHz

to 0.01 Hz. Water vapor permeability of the encapsulation materials was evaluated by following the ASTM test method E96. Washability tests were conducted by using a commercial laundry machine (3XWTW5905SW0, Whirlpool) and following AATCC Test Method 135. Briefly, TSC samples were put into a laundry bag and then the laundry bag was put into the laundry machine together with 1.8 kg fabrics serving as ballasts, followed by filling the washing machine with 72L of tap water. The delicate laundering mode was selected. In a typical laundry cycle, the agitator rotated at 27 strokes per minute for the washing and rinsing procedures. A spinning procedure with a spin speed of 500 rpm was finally carried out for about 5 min to remove the water. The entire laundering cycle lasted about 40 min. After laundering, the TSC was hanged to dry in the air before the electrochemical testing.

Calculation of the Electrochemical Performance of the TSC: The capacitance (C) calculated from CV and GCD curves were derived according to the equation $C = 0.5 \times S \times v^{-1} \times U^{-1}$ and $C = I \times t \times U^{-1}$, respectively. S is the whole integral area of the CV curve, v is the scan rate, U is the voltage window, I is the discharge current and t is the discharge time. The areal capacitance (C_A) was obtained according to $C_A = C \times A^{-1}$, where A is the projection area of the device including the composite yarn electrodes as well as the space between electrodes. The areal energy density (E_A) and power density (P_A) of the TSC were obtained from $E_A = C_A \times U^2 \times 7{,}200^{-1}$, $P_A = E_A \times 3{,}600 \times t^{-1}$.

Numerical simulation: A finite element method was employed to study the mechanical properties and interfacial behaviors of the TSCs made using different approaches. The simulation was performed in ABAQUS. The geometrical model for the AFEM-fabricated TSC (Model II) was comprised of the fabric substrate, fixing yarns, and the composite electrode yarn. Since electrode materials are not directly coated on the fabric substrate, the geometrical

structure of the fabric substrate in such an AFEM electrode model was simplified as a plane, in which the textile anisotropic property was still maintained to describe the deformation behavior of the fabric. Specifically, in this fabric substrate model, the textile anisotropic property was described by using 9 engineering constants Ei,j and $v_{i,j}$, where E and v are respectively the elastic modulus and Poisson ratio corresponding to the certain direction, and i,j=1,2,3 stands for the three directions. These 9 engineering constants are calculated by using the representative volume element (RVE) method and the TexGen software. As for the material properties of the fabric substrate, we referred to the experimental stress-strain properties presented in Figure 2c and Table S1. The fixing yarns were considered to be linearly elastic. For the composite electrode yarn, electrode materials were deposited around the fibers in the yarn. To mimic the composite electrode yarn and investigate the possible facture of the electrode materials in the composite electrode yarn, 19 twisted fibers (diameter: 30 μm) were firstly modeled to describe the electrode yarn configuration, and then the deposited electrode materials were modeled around the fibers. A material property with a higher Young's modulus than those of pristine textile materials was applied to the electrode materials layer, which could describe the property of the composite electrode materials. For the geometrical model of the TSC electrode (Model I) that were usually fabricated by the direct coating of electrode materials on fabric substrate, electrode materials were modeled on the fabric surface. As a control simulation, the material properties of the fabric substrate and electrode materials kept the same as those applied in Model II. In this model, the width of the electrode coated on the fabric substrate was the same as the diameter of composite electrode yarn in Model II, and the loading amount of electrode materials were also the same. Then the bending test was performed by applying a displacement at the edge of the fabric substrate, which could be further converted to the bending curvature (i.e., the reciprocal of the bending radius) of the sample. The magnitude of the von Mises stress and its distribution as well as the degree of fracture on the

electrode materials were then recorded, which were used to analyze the structural stability of the electrodes on the substrates made with different approaches.

Supporting Information
Supporting Information is available from the Wiley Online Library or from the author.

Acknowledgements
This work was supported by the General Research Fund of Hong Kong (PolyU 153032/18P) and The Hong Kong Polytechnic University (Project 1-YW0Z).

Received: ((will be filled in by the editorial staff))
Revised: ((will be filled in by the editorial staff))
Published online: ((will be filled in by the editorial staff))

References

[1] J. R. Miller, *Science* **2012**, *335*, 1312.
[2] S. Park; S. Jayaraman, *MRS Bull.* **2003**, *28*, 585.
[3] A. K. Yetisen; H. Qu; A. Manbachi; H. Butt; M. R. Dokmeci; J. P. Hinestroza; M. Skorobogatiy; A. Khademhosseini; S. H. Yun, *ACS Nano* **2016**, *10*, 3042.
[4] L. M. Castano; A. B. Flatau, *Smart Mater. Struct.* **2014**, *23*, 053001.
[5] K. Jost; G. Dion; Y. Gogotsi, *J. Mater. Chem. A* **2014**, *2*, 10776.
[6] Q. Y. Huang; D. R. Wang; Z. J. Zheng, *Adv. Energy Mater.* **2016**, *6*, 1600783.
[7] S. L. Zhang; N. Pan, *Adv. Energy Mater.* **2015**, *5*, 1401401.
[8] P. Simon; Y. Gogotsi, *Nat. Mater.* **2008**, *7*, 845.
[9] L. Hu; M. Pasta; F. La Mantia; L. Cui; S. Jeong; H. D. Deshazer; J. W. Choi; S. M. Han; Y. Cui, *Nano Lett.* **2010**, *10*, 708.
[10] J. Bae; M. K. Song; Y. J. Park; J. M. Kim; M. Liu; Z. L. Wang, *Angew. Chem. Int. Ed.* **2011**, *50*, 1683.
[11] L. Liu; Y. Yu; C. Yan; K. Li; Z. Zheng, *Nat. Commun.* **2015**, *6*, 7260.
[12] K. Jost; D. Stenger; C. R. Perez; J. K. McDonough; K. Lian; Y. Gogotsi; G. Dion, *Energy Environ. Sci.* **2013**, *6*, 2698.
[13] Y. Huang; H. Hu; Y. Huang; M. Zhu; W. Meng; C. Liu; Z. Pei; C. Hao; Z. Wang; C. Zhi, *ACS Nano* **2015**, *9*, 4766.
[14] L. Kou; T. Huang; B. Zheng; Y. Han; X. Zhao; K. Gopalsamy; H. Sun; C. Gao, *Nat. Commun.* **2014**, *5*, 3754.
[15] C. Choi; K. M. Kim; K. J. Kim; X. Lepro; G. M. Spinks; R. H. Baughman; S. J. Kim, *Nat. Commun.* **2016**, *7*, 13811.
[16] B. Wang; X. Fang; H. Sun; S. He; J. Ren; Y. Zhang; H. Peng, *Adv. Mater.* **2015**, *27*, 7854.
[17] Y. Yang; Q. Huang; L. Niu; D. Wang; C. Yan; Y. She; Z. Zheng, *Adv. Mater.* **2017**, *29*, 1606679.
[18] Z. S. Wu; K. Parvez; X. Feng; K. Mullen, *Nat. Commun.* **2013**, *4*, 2487.
[19] N. A. Kyeremateng; T. Brousse; D. Pech, *Nat. Nanotech.* **2017**, *12*, 7.
[20] D. Qi; Y. Liu; Z. Liu; L. Zhang; X. Chen, *Adv. Mater.* **2017**, *29*, 1602802.

[21] M. Zhu; Y. Huang; Y. Huang; H. Li; Z. Wang; Z. Pei; Q. Xue; H. Geng; C. Zhi, *Adv. Mater.* **2017**, *29*, 1605137.
[22] X. Pu; M. M. Liu; L. X. Li; S. C. Han; X. L. Li; C. Y. Jiang; C. H. Du; J. J. Luo; W. G. Hu; Z. L. Wang, *Adv. Energy Mater.* **2016**, *6*, 1601254.
[23] R. Guo; J. Chen; B. Yang; L. Liu; L. Su; B. Shen; X. Yan, *Adv. Funct. Mater.* **2017**, *27*, 1702394.
[24] S. S. Lee; K. H. Choi; S. H. Kim; S. Y. Lee, *Adv. Funct. Mater.* **2018**, *28*, 1705571.
[25] K. Dong; Y. C. Wang; J. Deng; Y. Dai; S. L. Zhang; H. Zou; B. Gu; B. Sun; Z. L. Wang, *ACS Nano* **2017**, *11*, 9490.
[26] G. Wang; V. Babaahmadi; N. He; Y. Liu; Q. Pan; M. Montazer; W. Gao, *J. Power Sources* **2017**, *367*, 34.
[27] S. Park; Y. G. Yoo; I. Nam; S. Bae; J. Yi, *Energy Technology* **2014**, *2*, 677.
[28] L. V. Thekkekara; M. Gu, *Sci. Rep.* **2019**, *9*, 11822.
[29] M. K. Jha; K. Hata; C. Subramaniam, *ACS Appl. Mater. Interfaces* **2019**, *11*, 18285.
[30] Y. Yu; C. Yan; Z. Zheng, *Adv. Mater.* **2014**, *26*, 5508.
[31] X. Q. Liu; H. X. Chang; Y. Li; W. T. S. Huck; Z. J. Zheng, *ACS Appl. Mater. Interfaces* **2010**, *2*, 529.
[32] D. R. Wang; Y. K. Zhang; X. Lu; Z. J. Ma; C. Xie; Z. J. Zheng, *Chem. Soc. Rev.* **2018**, *47*, 4611.
[33] H. Kim; J. Yoon; G. Lee; S. H. Paik; G. Choi; D. Kim; B. M. Kim; G. Zi; J. S. Ha, *ACS Appl. Mater. Interfaces* **2016**, *8*, 16016.
[34] Q. Huang; L. Liu; D. Wang; J. Liu; Z. Huang; Z. Zheng, *J. Mater. Chem. A* **2016**, *4*, 6802.
[35] L. Suo; O. Borodin; T. Gao; M. Olguin; J. Ho; X. Fan; C. Luo; C. Wang; K. Xu, *Science* **2015**, *350*, 938.
[36] G. Hasegawa; K. Kanamori; T. Kiyomura; H. Kurata; T. Abe; K. Nakanishi, *Chem. Mater.* **2016**, *28*, 3944.
[37] L. Zhang; D. DeArmond; N. T. Alvarez; R. Malik; N. Oslin; C. McConnell; P. K. Adusei; Y. Y. Hsieh; V. Shanov, *Small* **2017**, *13, 1603114*.
[38] J. Yun; D. Kim; G. Lee; J. S. Ha, *Carbon* **2014**, *79*, 156.
[39] B. Liu; B. Liu; X. Wang; D. Chen; Z. Fan; G. Shen, *Nano Energy* **2014**, *10*, 99.
[40] B. Liu; D. S. Tan; X. F. Wang; D. Chen; G. Z. Shen, *Small* **2013**, *9*, 1998.
[41] M. D. Lima; S. Fang; X. Lepro; C. Lewis; R. Ovalle-Robles; J. Carretero-Gonzalez; E. Castillo-Martinez; M. E. Kozlov; J. Oh; N. Rawat; C. S. Haines; M. H. Haque; V. Aare; S. Stoughton; A. A. Zakhidov; R. H. Baughman, *Science* **2011**, *331*, 51.

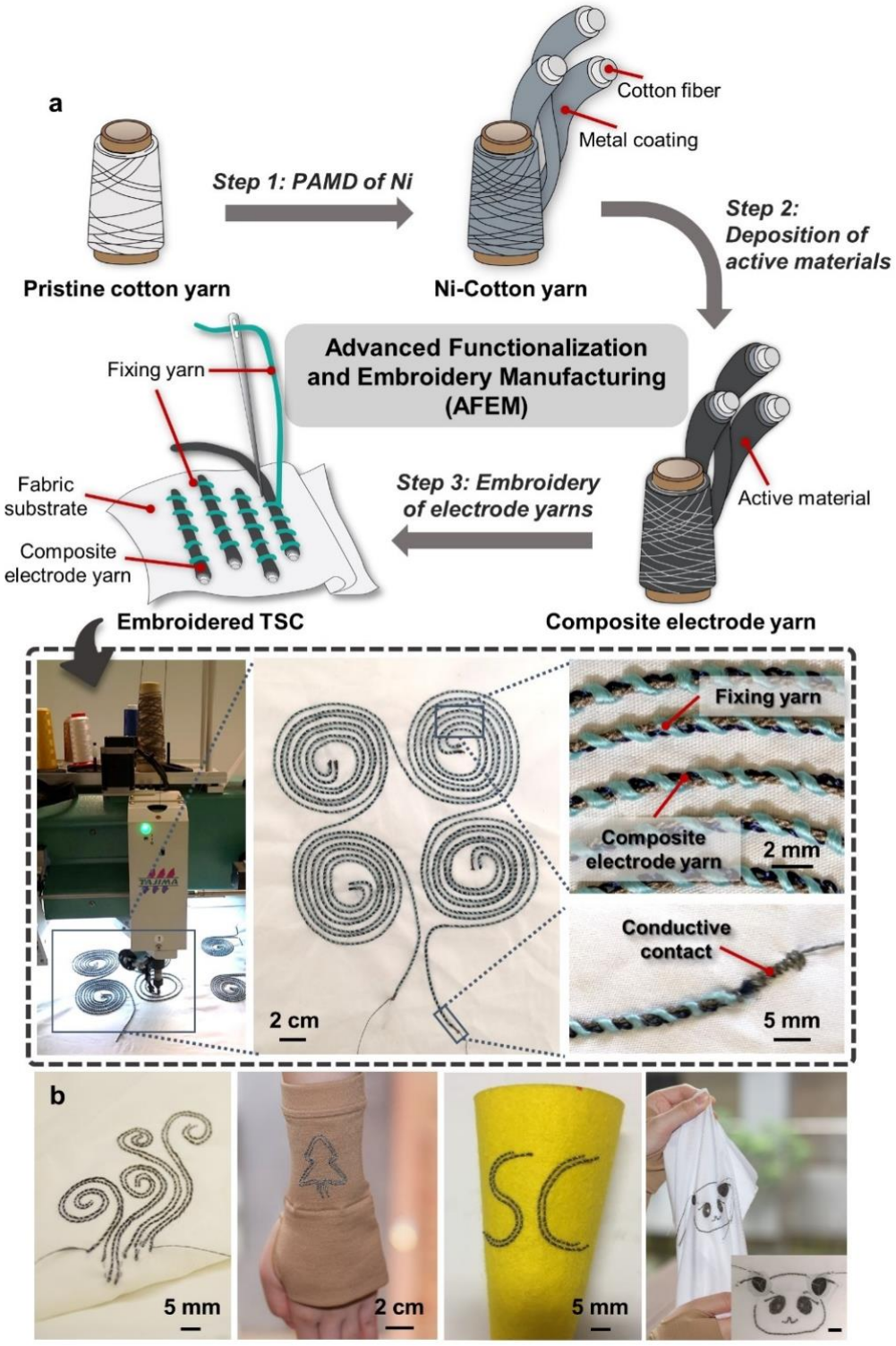

Figure 1. Fabrication processes of AFEM and TSC patterns. a) Schematic of the AFEM for the TSC. The figure inset shows a TAJIMA automatic embroidery machine was used to develop the wearable TSC fabric (Movie S1). The fabric includes four coil-shaped TSCs with an in-plane interdigitated electrode configuration and stitched conductive contact. b) Digital

images showing that the AFEM can be used to fabricate TSCs with different device patterns on different textile substrates. As demonstrations, in-plane SCs in coiled shape, tree shape, and letter shape (“SC”) were embroidered on woven, stretchable knitted, and non-woven fabrics (from left to right), respectively. A complicated panda-shaped pattern of TSCs was also made on the woven fabric, where the eyes and ears of the panda were four out-of-plane TSCs linked in series (scale bar: 1 cm).

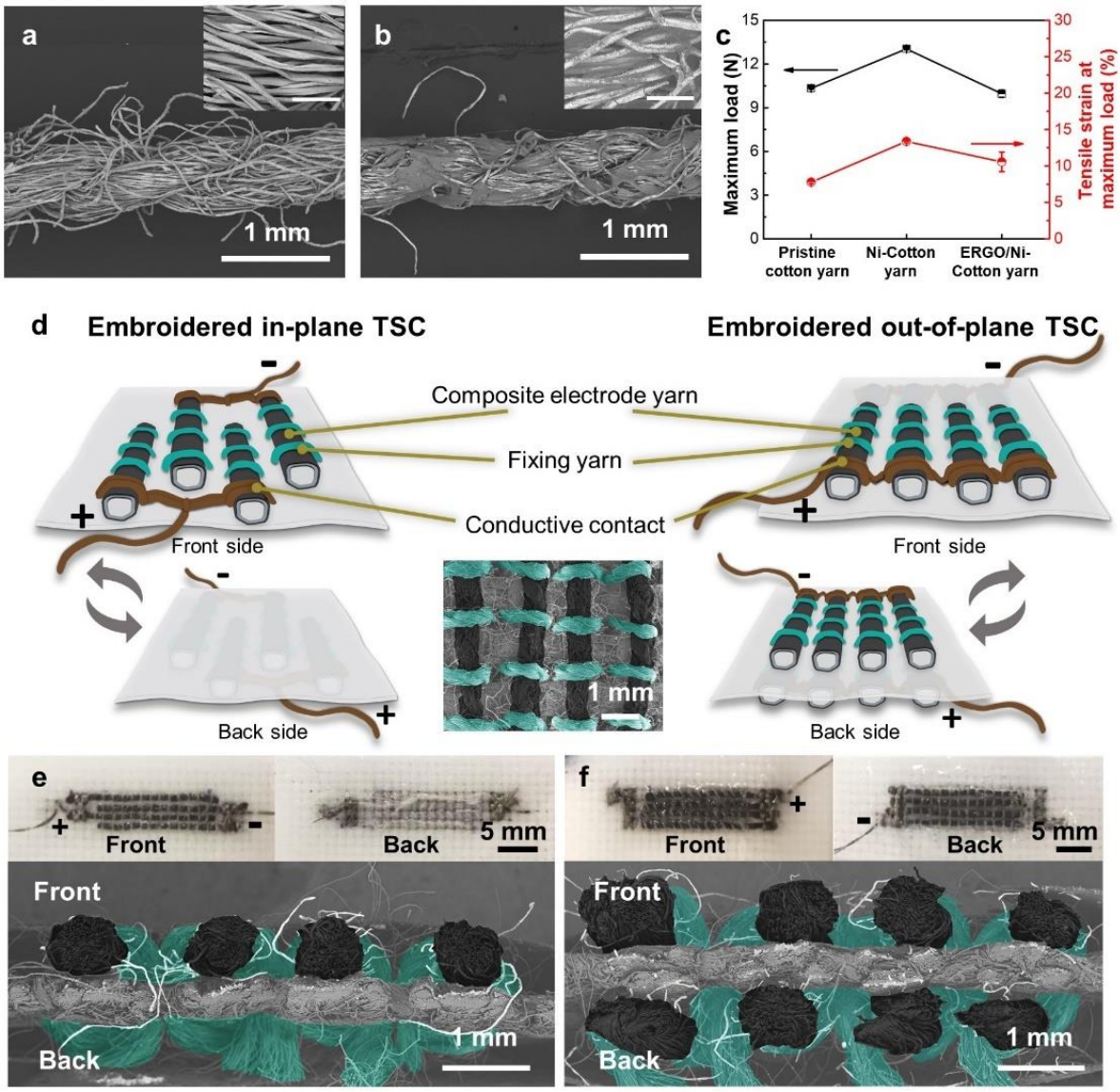

Figure 2. Structures of the composite electrode yarns and TSCs. a) Scanning electron microscopy (SEM) image of the Ni-Cotton cotton (Ni-Cotton) yarn. The inset is a high-resolution SEM image showing the Ni-Cotton fibers (scale bar: 150 μm). b) SEM image of the ERGO/Ni-Cotton composite electrode yarn. The inset is a high-resolution SEM image showing the ERGO/Ni-Cotton fibers (scale bar: 150 μm). c) Tensile properties of the Cotton yarn, Ni-Cotton yarn, and the ERGO/Ni-Cotton composite electrode yarn. d) Schematic diagrams of two different TSC structures achieved by in-plane embroidery (left) and out-of-plane embroidery (right), respectively. The inset is an SEM image showing the arrangement of composite electrode yarns in the embroidered TSC. e) Digital images (top) and SEM image

(bottom) showing the front, back and cross-sectional views of the in-plane TSC. f) Digital images (top) and SEM image (bottom) showing the front, back and cross-sectional views of the out-of-plane TSC.

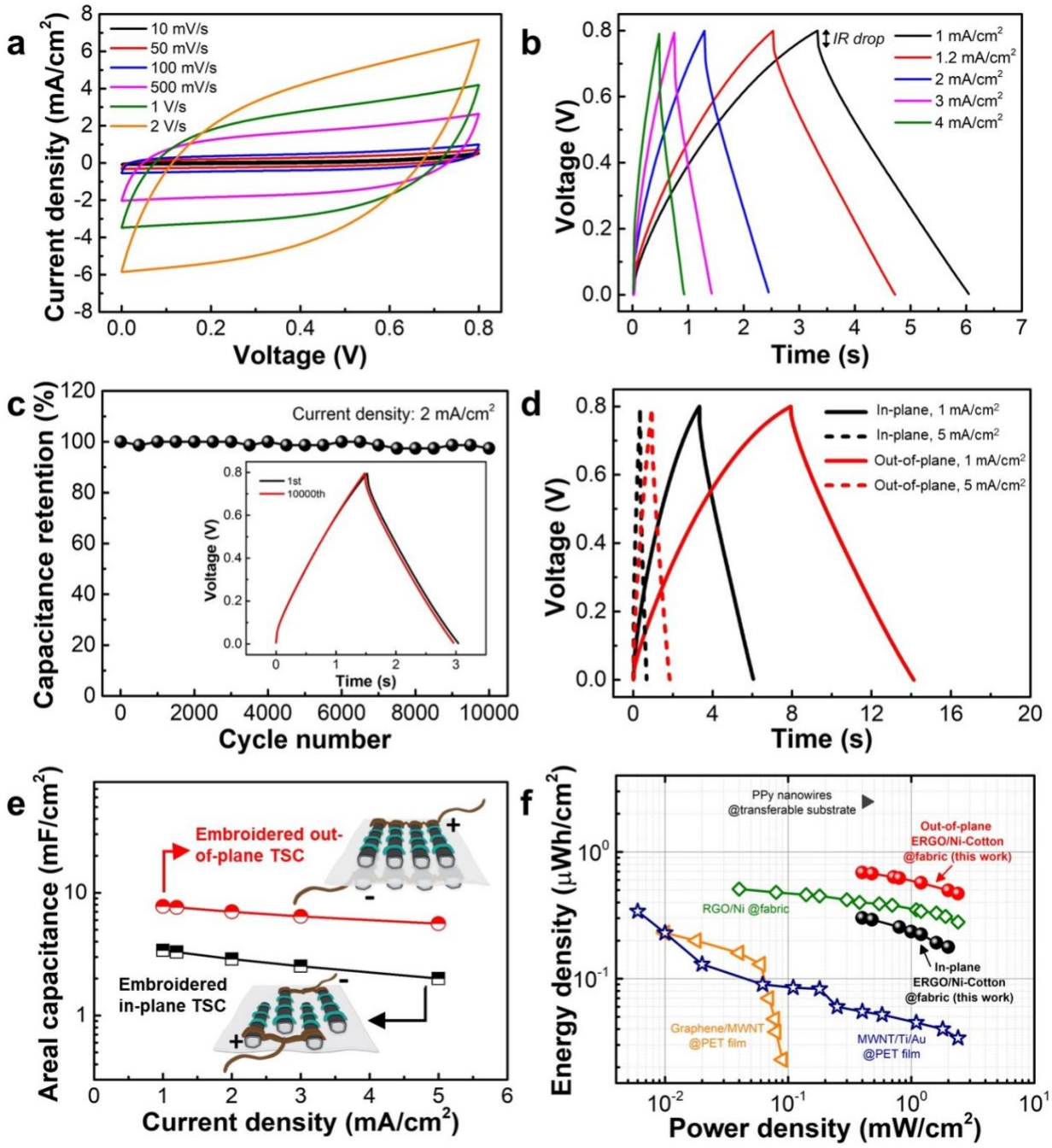

Figure 3. Electrochemical performance of TSCs. a) CV curves of the embroidered in-plane ERGO/Ni-Cotton TSC obtained at different scan rates. b) GCD curves of the embroidered in-plane ERGO/Ni-Cotton TSC measured at different current densities. c) Cycling performance of the embroidered in-plane TSC at a current density of 2 mA cm^{-2}. The inset shows GCD curves of a TSC before and after 10,000 charge/discharge cycles. d) GCD curves of the embroidered in-plane TSC and out-of-plane TSC measured at current densities of 1 and 5 mA

cm^{-2}, respectively. e) Summary of the areal capacitance of the embroidered in-plane and out-of-plane TSCs as a function of current density. f) Areal Ragone plot of the AFEM-fabricated TSC fabrics with in-plane and out-of-plane configurations, and other in-plane SCs made of polypyrrole (PPy) on transferable substrate[21], RGO/Ni on fabric[22], graphene/ MWNT on polyethylene terephthalate (PET) film[38], and MWNT/Ti/Au on PET film[33].

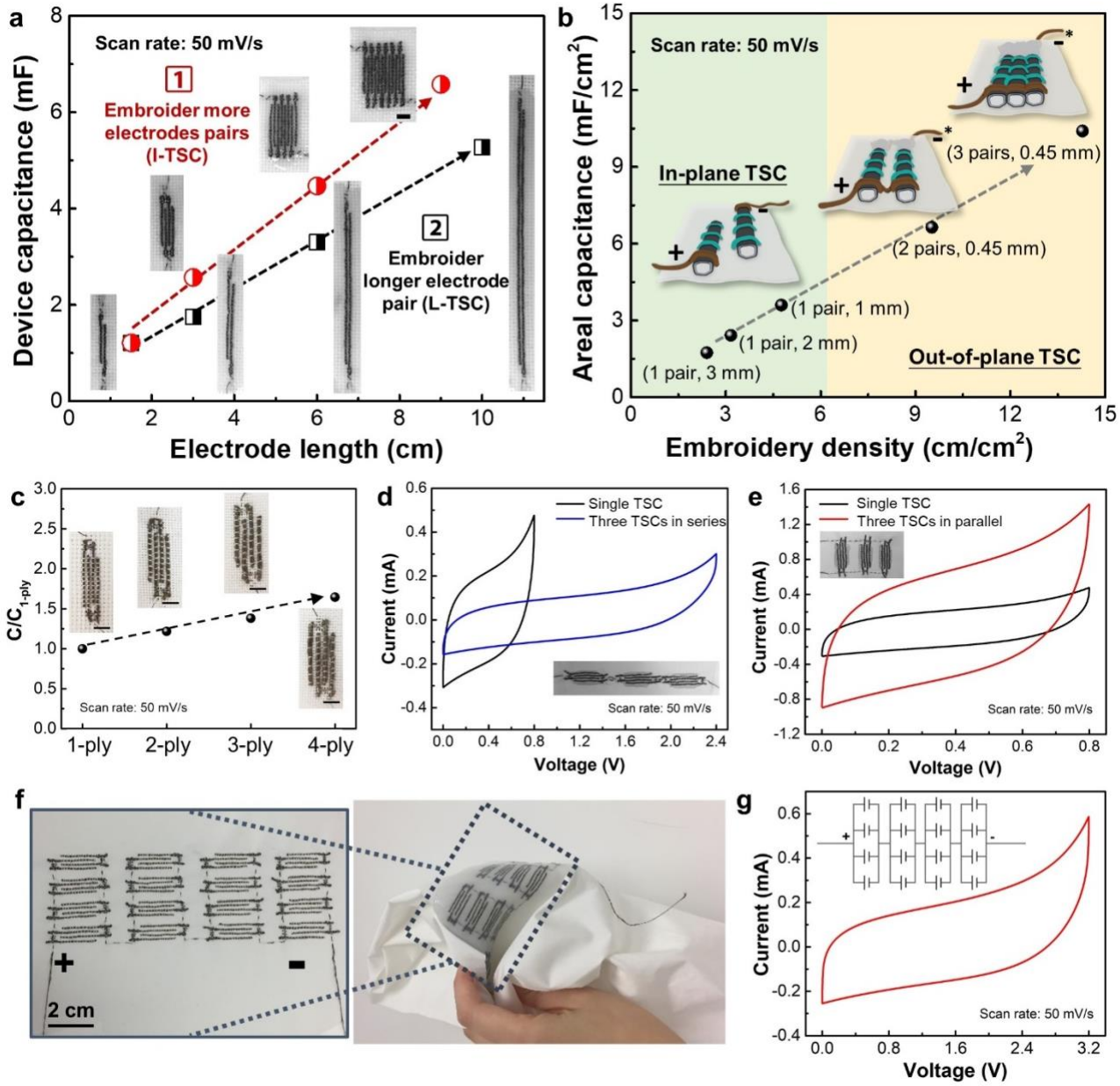

Figure 4. Tailorable fabrication of TSCs. a) Comparison of the dependence of areal capacitance on electrode yarn length for TSCs fabricated using two different scalable methods: (1) embroidering a long pair of electrode yarns (L-TSC) and (2) embroidering several electrode pairs to form interdigitated TSC (I-TSC). The insets are digital images of L-TSCs and I-TSCs (scale bar: 1 cm). b) Comparison of the areal capacitance of TSC as a function of embroidery density (i.e., the total length of electrode yarn in the specific area of the fabric). "(x_1 pair, x_2 mm)" indicates the number of the pairs of electrode yarns (x_1) and the gap distance between

the opposite electrode yarns (x_2). Capacitances for (a) and (b) were measured using a CV scan rate of 50 mV s^{-1}. c) Summary of the enhancement of the TSC device performance achieved by increasing the size of electrodes. "x-ply" describes that x yarns are plied together to form an electrode yarn. d) CV curves of three TSC units linked in series. Inset shows the digital image of the TSC in series. e) CV curves of three TSC units linked in parallel. Inset shows the digital image of the TSC in parallel. f) Digital images showing a piece of fabric consisting of 16 in-plane TSCs. Four devices in each column were connected in parallel and the 4 columns were connected in series. g) CV curve of the fabric with 16 in-plane TSCs. Inset shows the connection of 16 in-plane TSCs on the fabric. Through parallel and series connections, the output voltage of the TSC fabrics reached 3.2V.

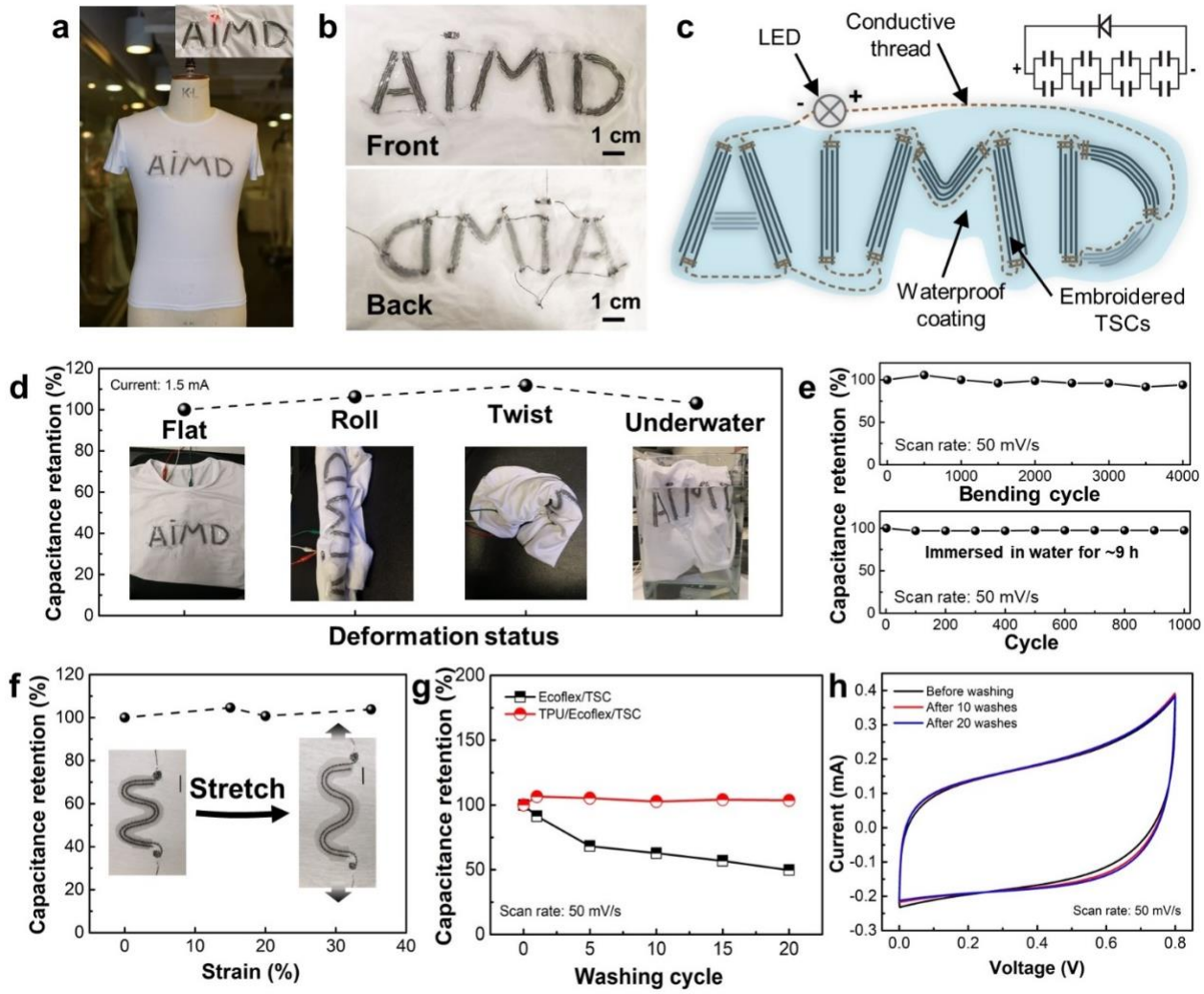

Figure 5. Wearable application of TSCs. a) Digital image of a T-shirt embroidered with TSCs and encapsulated with Ecoflex. b) Digital images showing the TSC pattern. c) Schematic illustration of the design of TSCs on the T-shirt. Black colored lines represent the TSCs embroidered as in-plane configuration, and brown colored lines represent the conductive contacts to connect each TSCs. d) Capacitance retention of the letter-shaped TSCs on the T-shirt under flat, rolling, twisting, and underwater conditions. e) Capacitance retention of the encapsulated TSC fabric after being bent for 4,000 cycles with a bending radius of 10 mm (top) and when tested underwater for up to 1,000 charge/discharge cycles (bottom). f) Capacitance retention of the in-plane TSC on the stretchable knitted fabric during the stretching. Inset shows the devices before and after stretching (scale bar: 1 cm). g) Comparison of the washability of

TSC fabrics encapsulated with Ecoflex and TPU fabric. h) CV curves of the Ecoflex and TPU fabric encapsulated TSC before and after washes.

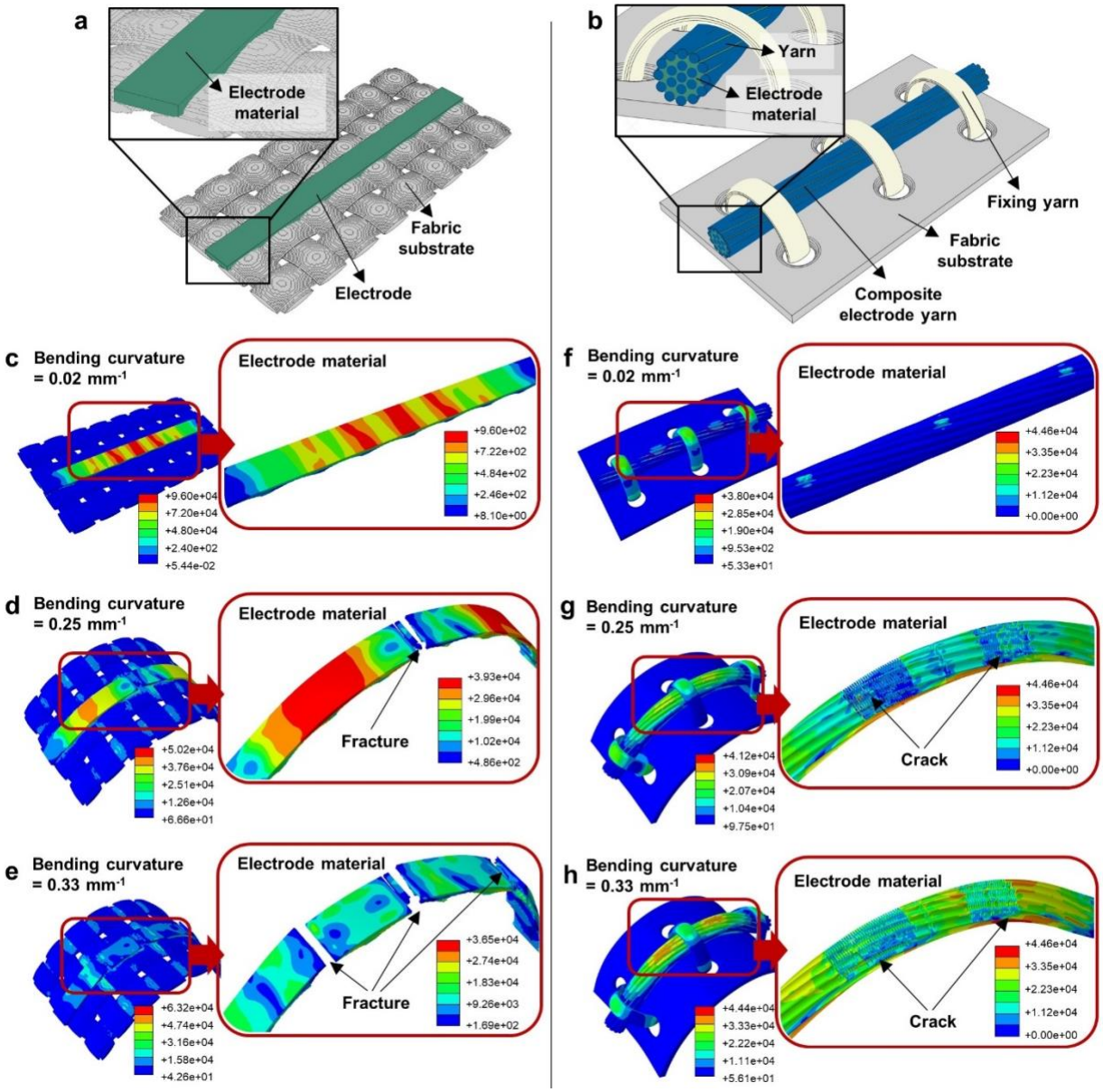

Figure 6. Schematic illustration showing the model design for Model I a) and Model II b). Model I mimicks the multi-layered structures of electrodes direcly coated on the fabric surface in the conventional fabrication of TSCs. Model II studied the embroided electrode structure by AFEM. Simulated diagrams of the distribution of von Mises stress in the bent electrode on Model I at the bending curvature of 0.02 mm^{-1} c), 0.25 mm^{-1} d), and 0.33 mm^{-1} e). Simulated diagram of the distribution of von Mises stress in the composite electrode yarn of a bent AFEM-fabricated TSC at the bending curvature of 0.02 mm^{-1} f), 0.25 mm^{-1} g), and 0.33 mm^{-1} h).

Table 1. Summary of the electrochemical performance of TSCs fabricated by AFEM using different device configurations, composite electrode yarns, and electrolytes.

TSCs	**Deposition method**	**Electrolyte**	**C (mF cm^{-2}) @ 10 mV/s**	**E (μWh cm^{-2})**	**P (mW cm^{-2})**
In-plane ERGO/Ni-Cotton@fabric	Electrochemical deposition	PVA/LiCl (0.8V)	5.34	0.30	2.0
		5m LiTFSI/H_2O (1.3V)	4.50	0.79	1.3
		20m LiTFSI/H_2O (1.5V)	3.53	0.48	1.1
Out-of-plane ERGO/Ni-Cotton@fabric		PVA/LiCl (0.8V)	10.38	0.69	2.4
In-plane DRGO/Ni-Cotton@fabric	Dip coating	PVA/LiCl (0.8V)	11.38	0.57	2.4
In-plane MWNT/Ni-Cotton@fabric	Wrapping	PVA/LiCl (0.8V)	15.75	1.29	2.0

Supporting Information

Additive Functionalization and Embroidery for Manufacturing Wearable and Washable Textile Supercapacitors

*Qiyao Huang, Dongrui Wang, Hong Hu, Jian Shang, Jian Chang, Chuan Xie, Yu Yang, Xavier Lepró, Ray H. Baughman, Zijian Zheng**

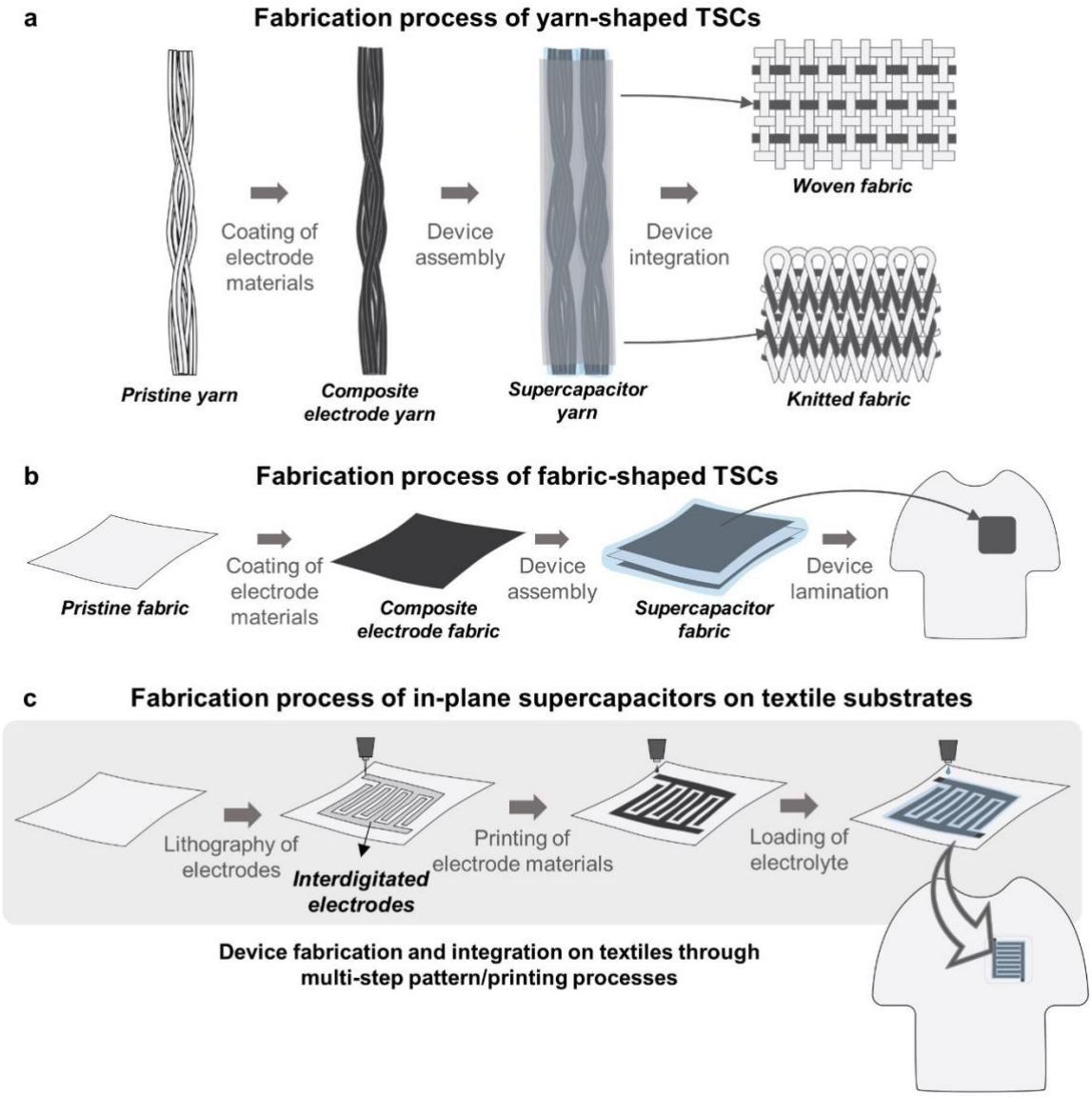

Figure S1. Schematic illustrations of the conventional fabrication processes of TSCs. Schematic illustrations showing the fabrication of yarn-shaped TSCs a), fabric-shaped TSCs b), and in-plane supercapacitors on textile substrates c) Conventional TSCs are usually fabricated ex-situ with a ply-yarn or multilayer-fabric structure and then integrated into the E-textile circuit by weaving, knitting or lamination technologies. In-plane supercapacitors are developed by multi-step patterning/printing processes. They are usually fabricated by the lithography of interdigitated electrodes on the textile surface, and then the printing or coating of functional materials on the patterned electrode surfaces.

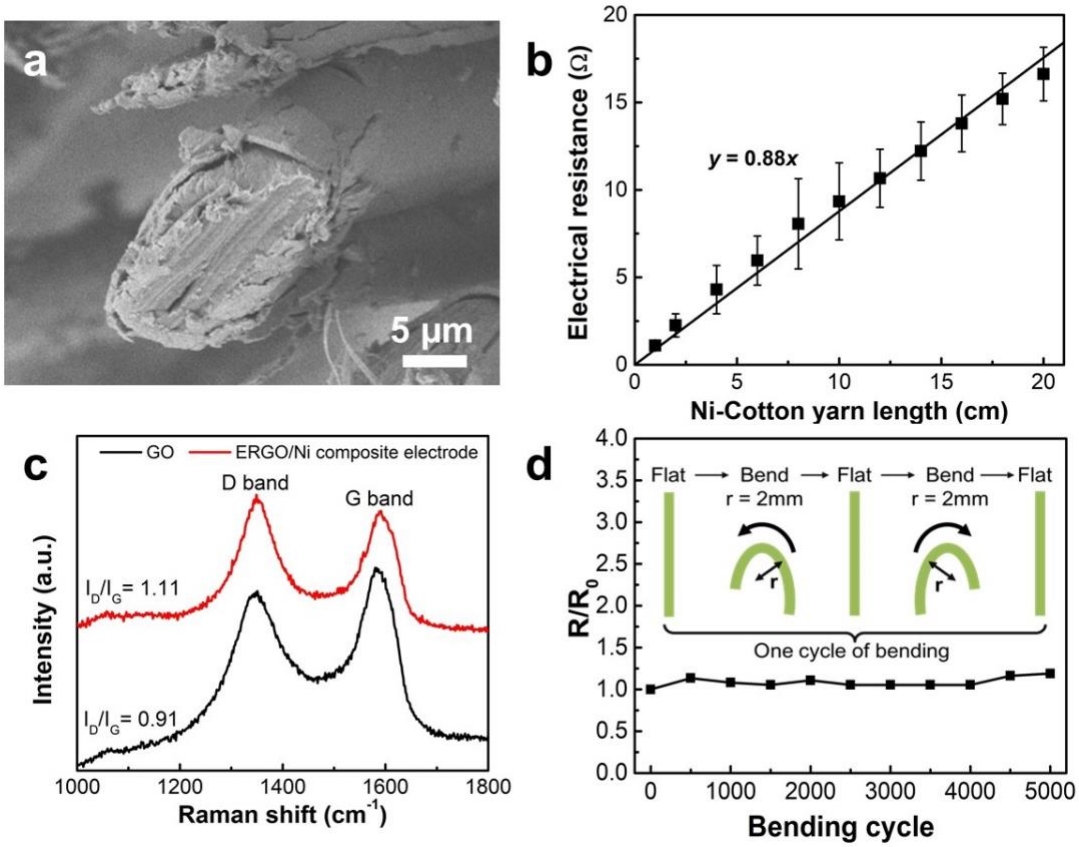

Figure S2. Characterization of the Ni-Cotton yarn and the ERGO/Ni-Cotton composite electrode yarn. a) SEM image of the cross-section of the Ni-Cotton yarn. b) Electrical resistance of the as-made Ni-Cotton yarn as a function of yarn length. c) Raman spectrum of the ERGO/Ni-Cotton composite electrode. The spectrum of ERGO/Ni-Cotton composite electrode shows an intensity ratio of D to G band (I_D/I_G) of 1.11, indicating the reduction of the GO (I_D/I_G = 0.91).[1] d) The yarn resistance (normalized to initial resistance) as a function of bending cycles to a bending radius of 2 mm.

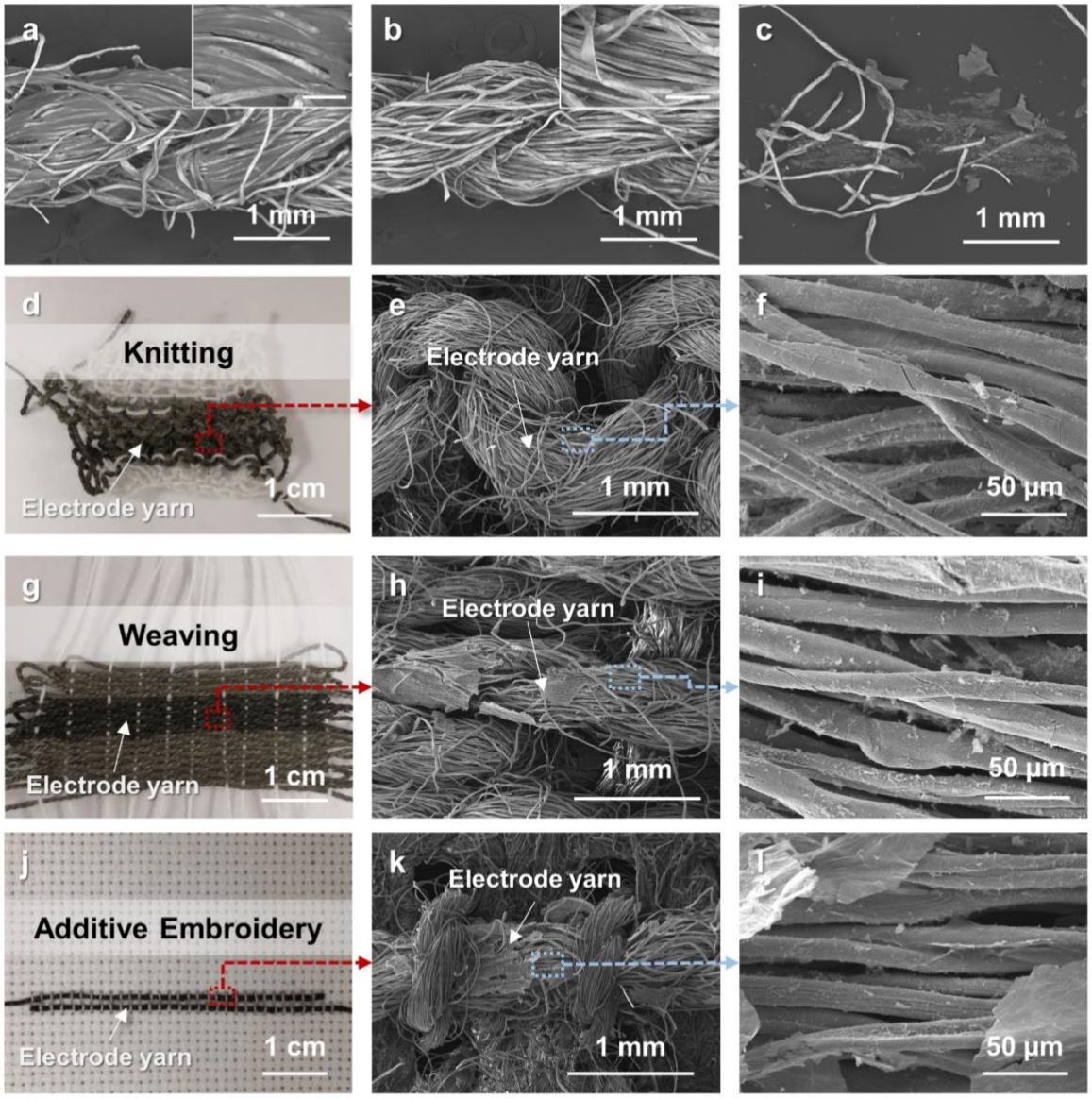

Figure S3. SEM images showing the composite electrode yarn before a) and after b) the pealing test, and the scotch tape c) adhered with RGO sheets from the electrode yarn surface. Digital images of fabrics with knitted d), woven g), and embroidered j) composite electrode yarns (in black color). SEM images of the electrode yarns after being knitted e)-f), woven h)-i), and embroidered k)-l) into fabrics.

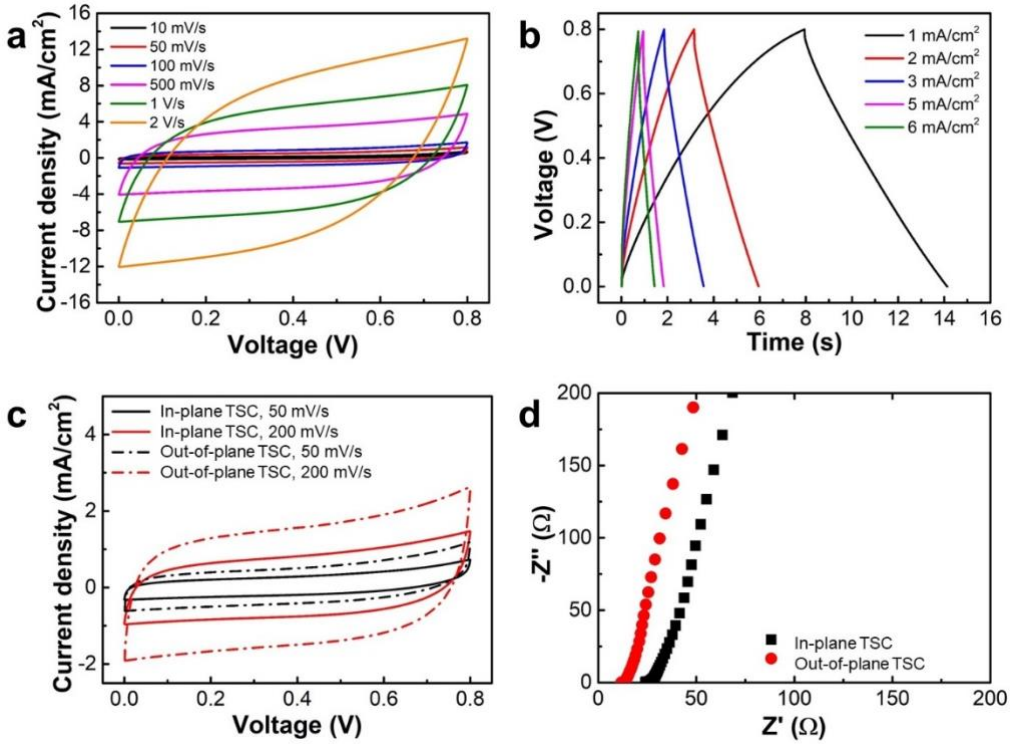

Figure S4. Electrochemical performance of the out-of-plane TSC. CV a) and GCD b) curves of the embroidered out-of-plane TSC with ERGO/Ni-Cotton electrodes. c) CV curves of the in-plane and out-of-plane TSCs measured at scan rates of 50 and 200 mV s^{-1}. d) AC impedance spectra of the in-plane and out-of-plane TSCs.

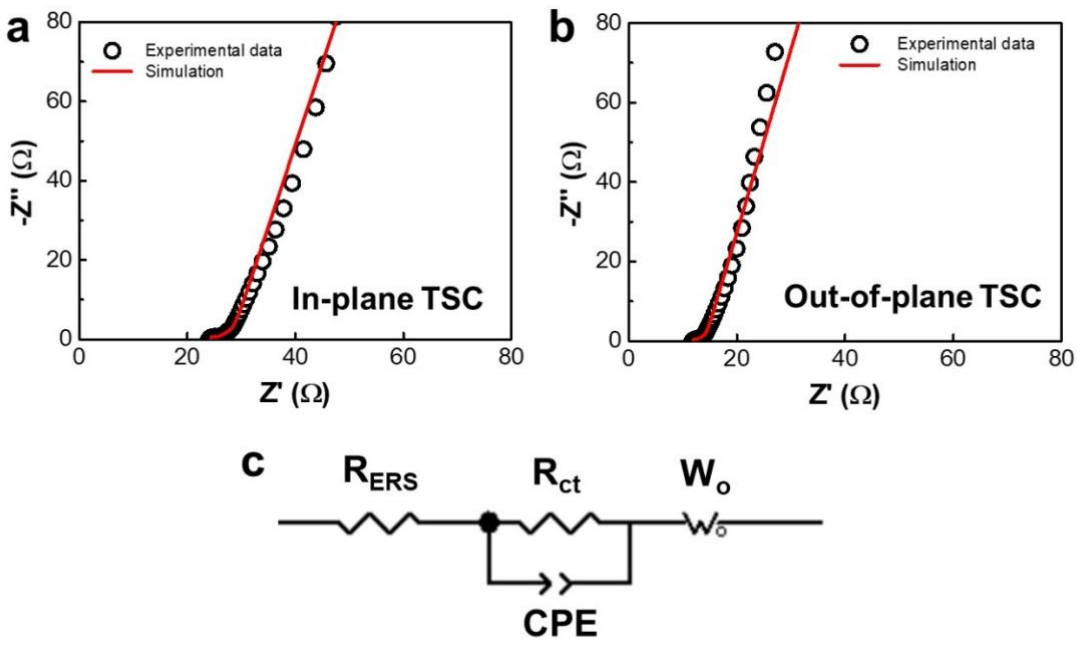

Figure S5. Nyquist plots for in-plane TSC a) and out-of-plane TSC b). The solid lines are the fitting simulation using the equivalent circuits in c). R_{ERS} is the equivalent series resistance (ESR), R_{ct} is the resistance of the electrode-electrolyte (charge transfer resistance), CPE is the electrical double layer capacitance, and Wo is the Warburg element (open).

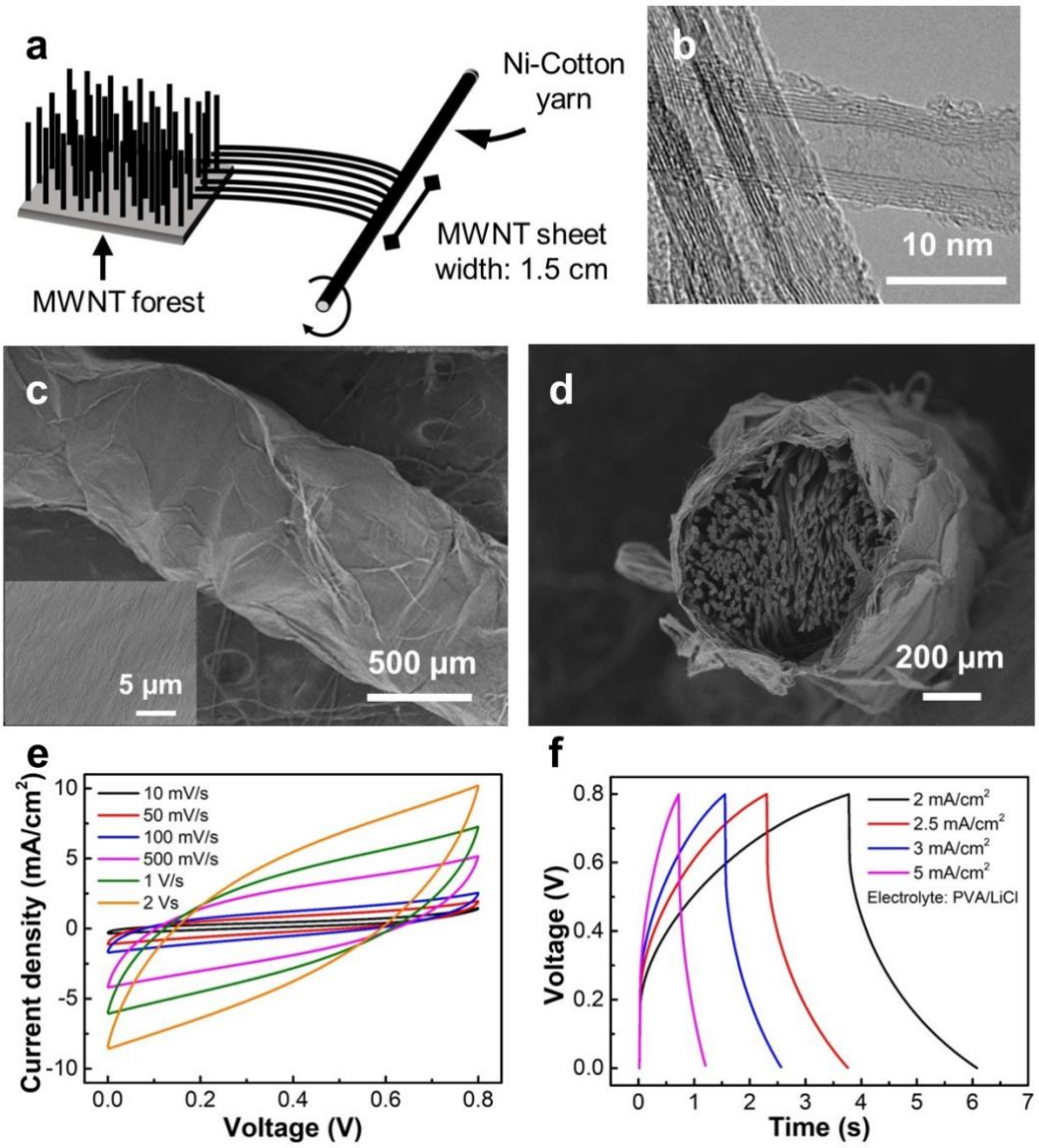

Figure S6. Characterization and electrochemical performance of the TSC with MWNT/Ni-Cotton composite electrode yarns. a) Schematic of the fabrication of the MWNT/Ni-Cotton composite electrode yarn. The electrode yarn is formed by wrapping the MWNT sheets (drawn from the MWNT forest) around the Ni-Cotton core yarn. b) Transmission electron microscopy (TEM) image of the MWNT nanofibers (diameter: ~9 nm) that are drawn from the MWNT forest. SEM images showing the longitudinal c) and cross-sectional d) morphologies of the MWNT/Ni-Cotton composite electrode yarn. The inset in c) is a high-resolution SEM image of MWNT films that were densely wrapped around the surface of Ni-Cotton yarn. CV e) and GCD f) of the in-plane MWNT/Ni-Cotton TSC.

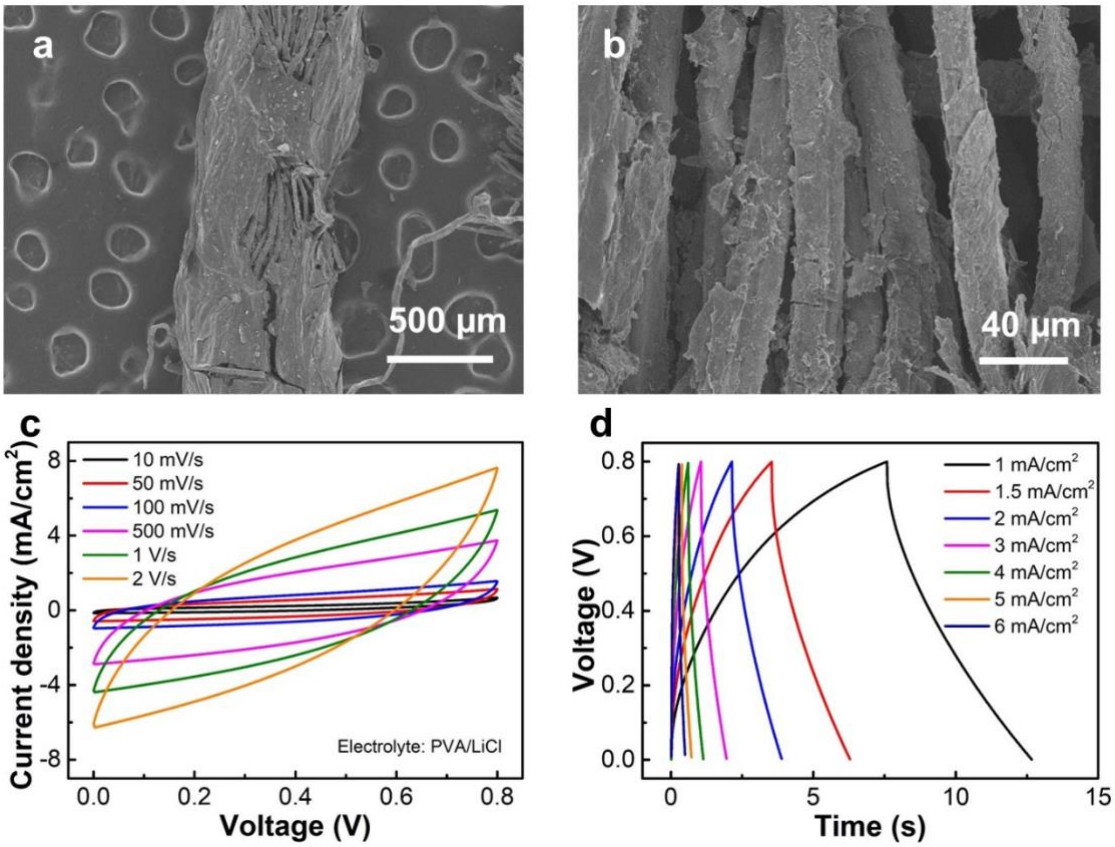

Figure S7. Characterization and electrochemical performance of the TSC with DRGO/Ni-Cotton composite electrode yarns. a) and b) SEM images showing the morphology of the DRGO/Ni-Cotton composite electrode yarn. The DRGO/Ni-Cotton composite electrode yarn was fabricated by dip-coating and chemical reduction of the graphene oxide (DRGO) on the Ni-Cotton yarn. CV c) and GCD d) curves of the embroidered in-plane DRGO/Ni-Cotton TSC.

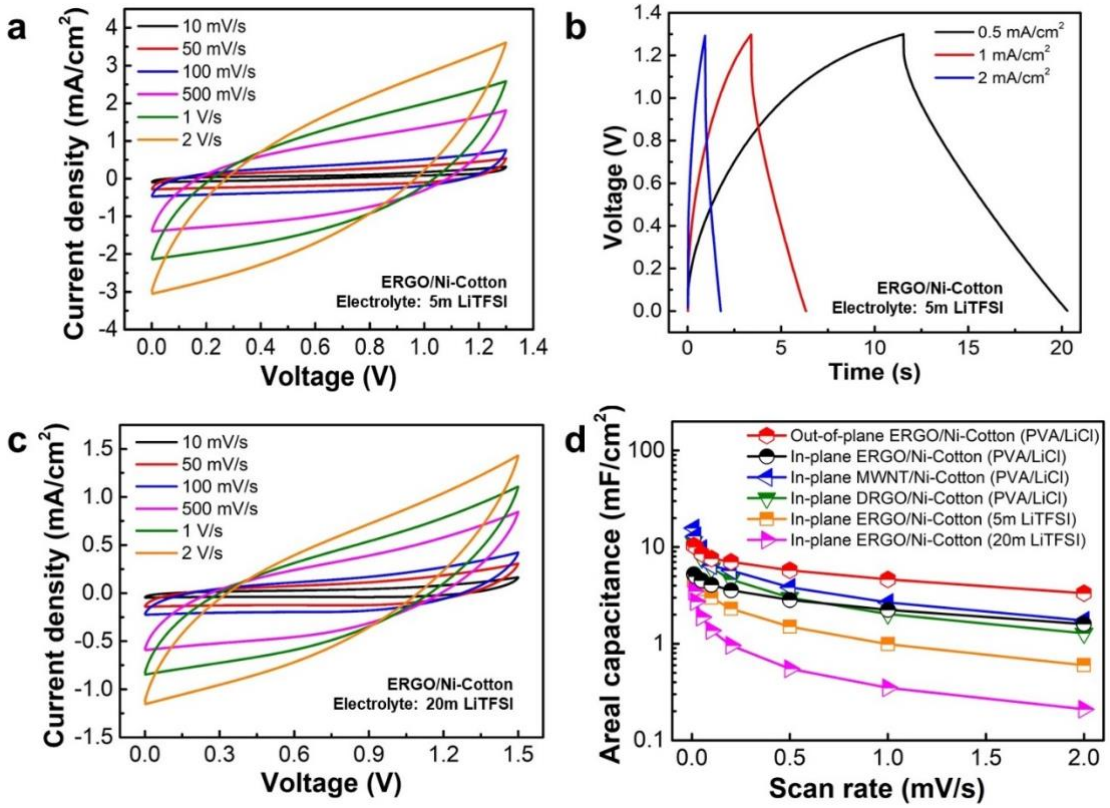

Figure S8. Electrochemical performance of the TSCs with different composite electrode yarns and electrolytes. CV a) and GCD b) curves of the in-plane ERGO/Ni-Cotton TSC (electrolyte: 5 m LiTFSI) at different scan rates. c) CV curves of the in-plane ERGO/Ni-Cotton TSC (electrolyte: 20 m LiTFSI) at different scan rates. By using 5 m (i.e., 5 mol of LiTFSI in 1 kg of deionized water), the voltage window could be extended to 1.3 V. Further increase of the electrolyte concentration could lead to a wider voltage window of up to 1.5 V. This is because the high concentration of LiTFSI in water can not only reduce water activity and modulate redox potentials but can also suppress hydrogen evolution.[2-3] d) Summary of the areal capacitance of the as-embroidered TSCs with different device configurations, composite electrode yarns, and electrolytes. Although using "water-in-salt" electrolytes (i.e., 5 m and 20 m LiTFSI) could extend the voltage window of SC devices, the capacitance performance was sacrificed. This may be because of the bulky TFSI anion and the poor ionic conductivity of LiTFSI compared to the "salt-in-water" electrolyte (i.e., PVA/LiCl).[4]

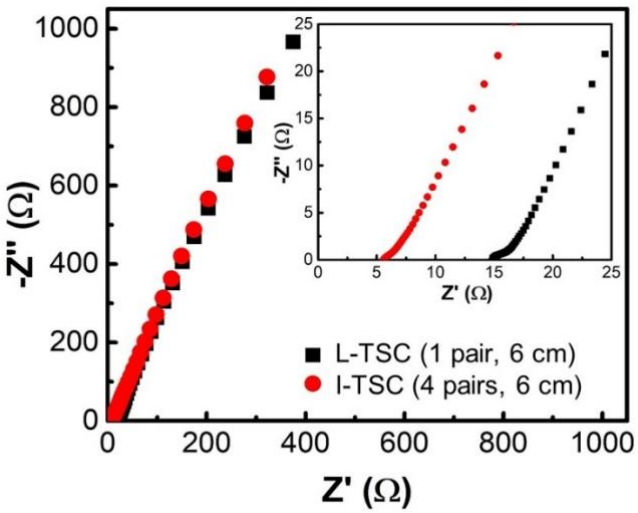

Figure S9. AC impedance spectra of the L-TSC and I-TSC with the same length of electrode yarns (6 cm).

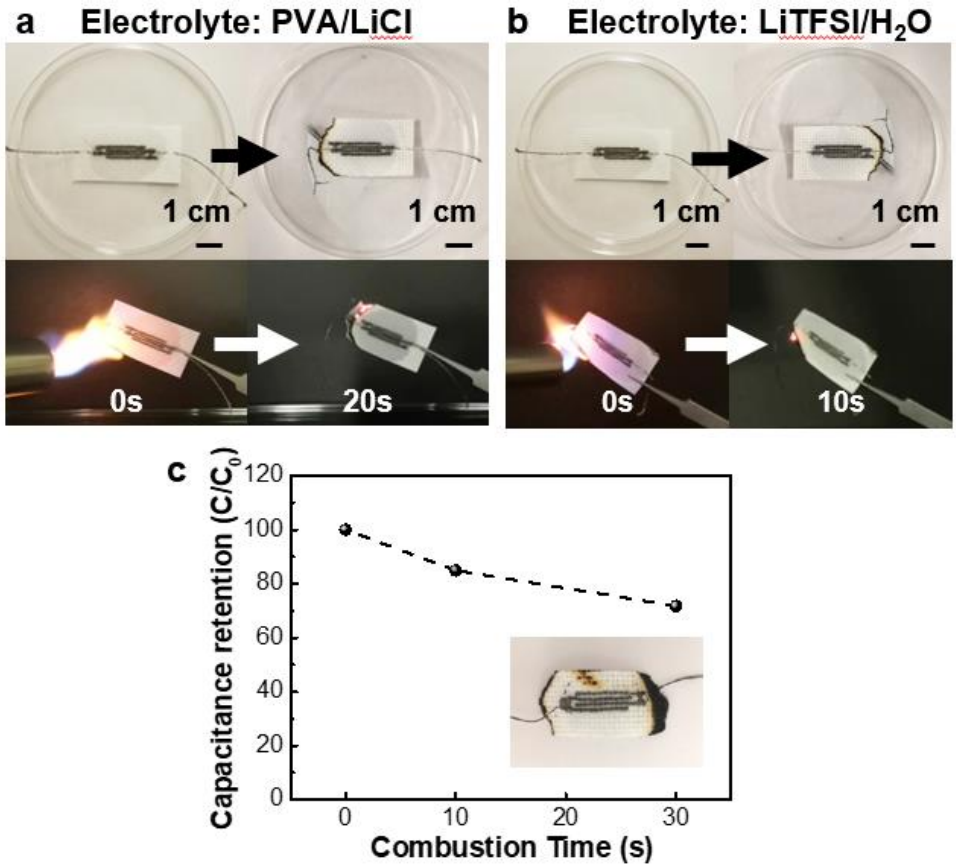

Figure S10. Fire-retardant test of the TSCs with different aqueous electrolytes. Digital images showing the TSCs with PVA/LiCl a) and LiTFSI b) as electrolytes before (left) and after (right) fire-retardant test. The flame gradually extinguished when approaching the device area, indicating the non-flammability of the electrolytes. c) Capacitance retention of the in-plane TSC with the increase of the combustion time.

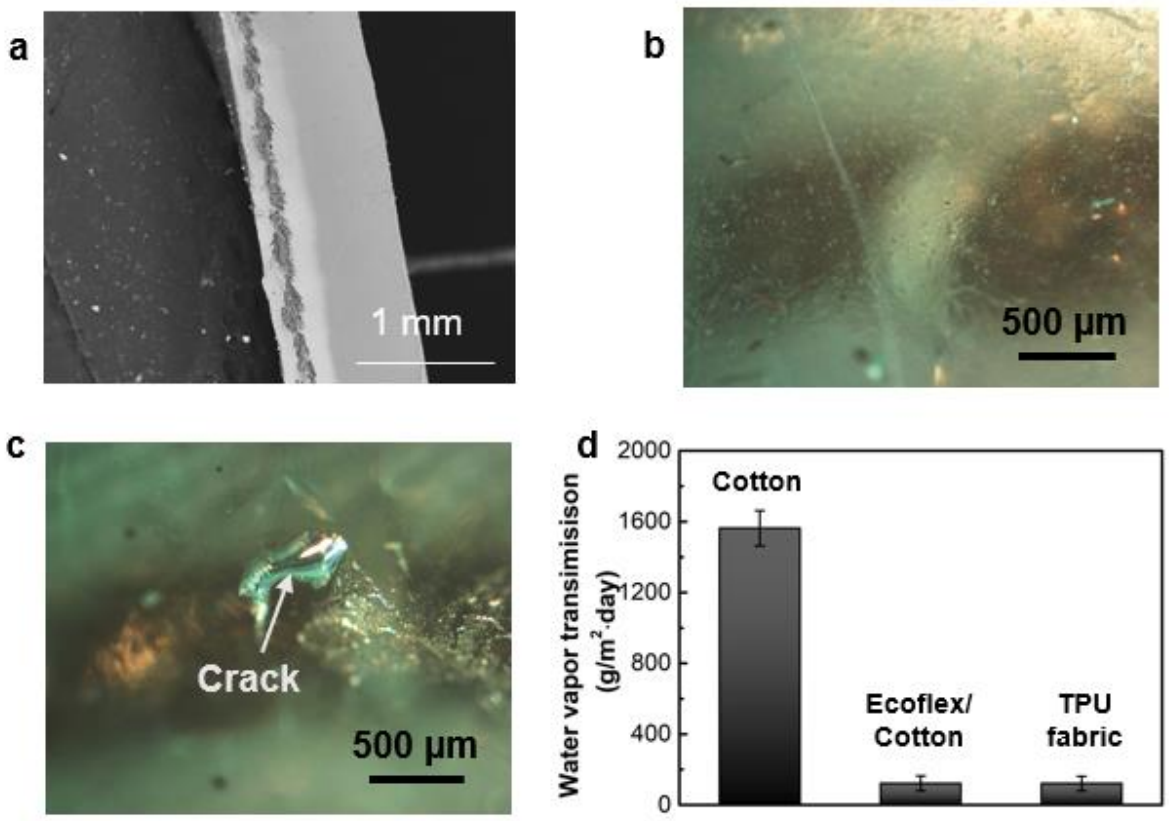

Figure S11. a) SEM image showing the cross-section of the TSC fabric firmly encapsulated with the Ecoflex. When Ecoflex was coated on the top and bottom side of the device area in the fabric, the coating filtrated into the gaps between fibers within the fabric. As a result, the device can be firmly sealed. Optical microscopic image showing the Ecoflex film covered on the surface of the TSC area b) and the crack on the Ecoflex film surface after 20 washes c). d) Water vapor transmission of the cotton fabric substrate, Ecoflex-coated cotton substrate (Ecoflex/cotton) and TPU fabric. Lower water vapor transmission value indicates the low water vapor permeability of the materials.

Table S1 Summary of the tensile properties of the yarns before and after the additive functionalization of electrode materials.

Yarn	**Pristine cotton yarn**	**Ni-Cotton yarn**	**RGO/Ni-Cotton yarn**
Maximum load (N)	10.3	13.0	10.0
Tensile strain at maximum load (%)	7.8	13.4	10.6
Young's modulus (MPa)	89	96	213

Table S2. Comparison of the electrochemical performance of embroidered TSC (this study) and the previously reported in-plane supercapacitors.

SCs	Patterning method	Electrolyte	C ($mF\ cm^{-2}$)	E ($\mu Wh\ cm^{-2}$)	P ($mW\ cm^{-2}$)
Embroidered TSCs (This work)	AFEM (in-plane / out-of-plane embroidery)	PVA/LiCl (0.8V) or LiTFSI (1.3~1.5V)	3.53 ~ 15.75	0.30 ~ 1.29	1.1 ~ 2.4
RGO/Ni@fabric[5]	Mask-assisted deposition	PVA/H_3PO_4	8.19	0.51	2.4
MWNT/Au@PET[a] film[6]	Photolithography	PEGDA/ [EMIM][TFSI][b] (1.5V)	0.51	0.34	2.4
MnO_2/Ni@Paper[7]	Screen printing	CMC[c]/Na_2SO_4 (0.8V)	2.18	0.19	3.58
Graphene/Kapton film[8]	Laser engraving	PVA/H_2SO_4 (1V)	2.4	0.38	14.4
PPy[d] nanowires@transferable substrate[9]	Commercial etching process	PVA/H_3PO_4 (0.5V)	8.15	0.43	2.49
Graphene/MWNT@PET film[10]	Photolithography	PVA/H_3PO_4 (0.8V)	2.54	0.23	0.09
LGO[e]/Au@PET fabric[11]	Laser scribing	PVA/H_2SO_4 (1V)	0.756	0.042	1.12

[a] PET: polyethylene terephthalate; [b] PEGDA/[EMIM][TFIS]: poly(ethylene glycol) diacrylate/1-ethyl-3-methylimidazolium bis(trifluoromethylsulfonyl)imide; [c] CMC: Carboxymethyl cellulose; [d] Ppy: Polypyrrole; [e] LCO: laser-scribed graphene oxide

Table S3. Mass loading of the active materials on different composite electrode yarns.

Composite electrode yarns	ERGO/Ni-Cotton yarn	DRGO/Ni-Cotton yarn	MWNT/Ni-Cotton yarn
Mass loading of active materials (mg cm^{-1})	0.17	0.22	0.03

Reference

[1] L. Liu; Y. Yu; C. Yan; K. Li; Z. Zheng, *Nat. Commun.* **2015**, *6*, 7260.
[2] M. Zhang; S. Makino; D. Mochizuki; W. Sugimoto, *J. Power Sources* **2018**, *396*, 498.
[3] L. Suo; O. Borodin; T. Gao; M. Olguin; J. Ho; X. Fan; C. Luo; C. Wang; K. Xu, *Science* **2015**, *350*, 938.
[4] A. Gambou-Bosca; D. Bélanger, *J. Power Sources* **2016**, *326*, 595.
[5] X. Pu; M. M. Liu; L. X. Li; S. C. Han; X. L. Li; C. Y. Jiang; C. H. Du; J. J. Luo; W. G. Hu; Z. L. Wang, *Adv. Energy Mater.* **2016**, *6*, 1601254.
[6] H. Kim; J. Yoon; G. Lee; S. H. Paik; G. Choi; D. Kim; B. M. Kim; G. Zi; J. S. Ha, *ACS Appl. Mater. Interfaces* **2016**, *8*, 16016.
[7] R. Guo; J. Chen; B. Yang; L. Liu; L. Su; B. Shen; X. Yan, *Adv. Funct. Mater.* **2017**, *27*, 1702394.
[8] L. Zhang; D. DeArmond; N. T. Alvarez; R. Malik; N. Oslin; C. McConnell; P. K. Adusei; Y. Y. Hsieh; V. Shanov, *Small* **2017**, *13*, *1603114*.
[9] M. Zhu; Y. Huang; Y. Huang; H. Li; Z. Wang; Z. Pei; Q. Xue; H. Geng; C. Zhi, *Adv. Mater.* **2017**, *29*, 1605137.
[10] J. Yun; D. Kim; G. Lee; J. S. Ha, *Carbon* **2014**, *79*, 156.
[11] G. Wang; V. Babaahmadi; N. He; Y. Liu; Q. Pan; M. Montazer; W. Gao, *J. Power Sources* **2017**, *367*, 34.